https://doi.org/10.5194/egusphere-2026-4135
Preprint. Discussion started: 22 July 2026

Quasi-Biennial Oscillation Modulation of the Semi-Annual Oscillation in QBOi Models

Aleena M. Jaison[1,2], Lesley J. Gray[1,3], Scott Osprey[1,3], James A. Anstey[4], Martin B. Andrews[5], Neal Butchart[5], Zhaoyang Chai[6], Dong-Chan Hong[7], Kai Huang[8], Yoshio Kawatani[9], Jeff R. Knight[5], Pu Lin[10,11], Francois Lott[12], Yixiong Lu[13], Hiroaki Naoe[14], Jadwiga H. Richter[8], Nan Rosenbloom[8], Federico Serva[15], Anne K. Smith[8], Seok-Woo Son[7], Qi Tang[16], Shingo Watanabe[17,18], Jinbo Xie[16,19], and Kohei Yoshida[14]

[1]Atmospheric, Oceanic and Planetary Physics, University of Oxford
[2]Space, Plasma and Climate, Imperial College London
[3]National Centre for Atmospheric Science, Oxford, United Kingdom
[4]Canadian Centre for Climate Modelling and Analysis (CCCma), Victoria, Canada
[5]Met Office Hadley Centre (MOHC), Exeter, UK
[6]Institute of Atmospheric Physics, Chinese Academy of Sciences (CAS), Beijing, China
[7]School of Earth and Environmental Sciences, Seoul National University, Seoul, 08826, Korea
[8]National Science Foundation National Center for Atmospheric Research, Boulder, CO, 80305, USA
[9]Faculty of Environmental Earth Science, Hokkaido University, Sapporo, Japan
[10]NOAA Geophysical Fluid Dynamics Laboratory, Princeton, NJ, USA
[11]Boston College, Chestnut Hill, MA, USA
[12]Laboratoire de Météorologie Dynamique (LMD), Paris, France
[13]State Key Laboratory of Severe Weather Meteorological Science and Technology, Earth System Modeling and Prediction Centre, China Meteorological Administration, Beijing, China
[14]Meteorological Research Institute (MRI), Tsukuba, Japan
[15]Institute of Marine Sciences, National Research Council (CNR-ISMAR), Rome, Italy
[16]Lawrence Livermore National Laboratory, Livermore, CA, USA
[17]Japan Agency for Marine-Earth Science and Technology (JAMSTEC), Yokohama, Japan
[18]Advanced Institute for Marine Ecosystem Change (WPI-AIMEC), Tohoku University, Sendai, Japan
[19]High Meadows Environmental Institute (HMEI), Princeton University, Princeton, NJ, USA

Correspondence to: Aleena M. Jaison (a.moolakkunnel-jaison@imperial.ac.uk)

https://doi.org/10.5194/egusphere-2026-4135
Preprint. Discussion started: 22 July 2026

Abstract. As part of the Quasi-Biennial Oscillation initiative (QBOi) phase 1, a model-intercomparison study explored the representation of the semi-annual oscillation (SAO) in participating models and found a common easterly bias of several tens of m/s compared to observations, mostly with weaker westerly phases and stronger easterly phases. QBOi phase 1 results also reported biases in model representations of the QBO, which dominates the region below the SAO, with most models displaying a westerly time mean wind bias, and generally weaker QBO easterly phases. Given that the SAO forcing terms can be influenced by the QBO, in this paper we explore the influence of these QBO biases on the representation of the SAO. A multi-model analysis is conducted here using QBOi phase 2 data from current state-of-the-art climate models to examine changes in representation of the SAO in response to corrections in zonal-mean zonal wind QBO biases. Most models show an improvement with a reduced easterly SAO bias in response to the corrected QBO bias. The extent of this response is found to vary significantly across models with SAO time-mean winds changing by 6% to 403% in simulations with a bias-corrected QBO relative to the control simulations. Changed gravity wave drag in response to the improved QBO is attributed as the forcing term having the largest overall impact.

1 Introduction

Periodically alternating zonal-mean zonal winds represent the dominant mode of atmospheric variability in the equatorial stratosphere. The quasi-biennial oscillation (QBO), occurring in the lower to middle stratosphere, exhibits alternating zonal-mean westerlies and easterlies with a mean periodicity of 28 months, while the stratospheric semi-annual oscillation (SAO) dominates the upper stratosphere with a periodicity of 6 months. Although these oscillations are confined to the equatorial stratosphere they have been shown to significantly impact the extra-tropics (Andrews et al., 2019; Baldwin et al., 2001; Gray et al., 2020).

The SAO wind oscillations primarily occur between 5 hPa to 0.3 hPa, reaching peak magnitudes around 1 hPa. SAO easterlies appear during solstices with peak speeds of approximately 30m/s, while westerlies dominate during the equinoxes, reaching up to 40m/s. Meridional advection associated with the Brewer-Dobson circulation (BDC) is the primary driver of the easterly SAO phase. The BDC advects summer hemisphere easterlies across the equator into the winter hemisphere, thus explaining why the easterlies tend to appear at a range of altitude at the same time (between 0.3–5 hPa) (Holton and Wehrbein, 1980). Extra-tropical quasi-stationary waves are also suggested to transfer momentum to this phase (Hopkins, 1975). Although earlier works suggested a minor role for vertically propagating easterly gravity waves in driving the easterly SAO phase, the evidence remain limited and no widely supported relationship has been identified (Antonita et al., 2007; Deepa et al., 2006; Ray et al., 1998). The westerly phase, on the other hand, is mainly driven by vertically propagating equatorial waves, such as gravity waves and Kelvin waves, and exhibits shear descent over time (Hirota, 1978; Hitchman and Leovy, 1988). The SAO also displays intra-annual variation with the easterly phase during Northern Hemisphere (NH)

https://doi.org/10.5194/egusphere-2026-4135
Preprint. Discussion started: 22 July 2026

winter months being stronger than during the Southern Hemisphere (SH) winter (Delisi and Dunkerton, 1988; Quiroz and Miller, 1967).

The first identification of the SAO was by Reed (1966), using rocket sonde observations at Ascension Island and Barking Sands. Later, Garcia et al. (1997) and Ray et al. (1998) showed the SAO in zonal-mean zonal wind from wind observations made by the High Resolution Doppler Imager (HRDI). However, altitudes from roughly 2 hPa to 0.1 hPa were not examined due to data scarcity. While direct observations in the upper stratosphere remain sparse, presenting difficulties to studying the SAO, alternative approaches have been employed. Recently, Smith et al., (2017), using satellite retrievals of geopotential heights from the Sounding of the Atmosphere using Broadband Emission Radiometry (SABER) and Microwave Limb Sounder (MLS), derived monthly and zonally averaged winds in the upper stratosphere based on reasonable gradient wind balance assumptions, and presented the climatology of SAO from almost 15 years of data. Reanalysis models do not generally assimilate observational data at SAO altitudes and thus show substantial variations in their ability to represent the SAO (Kawatani et al., 2020). However, reanalyses that most resemble the SAO in observations have been used to examine the characteristics of the SAO and its forcing mechanisms (Ern et al., 2021; Jaison et al., 2024a)

Climate model simulations of the SAO suffer from significant biases. Early studies such as Meyer (1970) and Holton and Wehrbein (1980) explored the SAO using simplified models and were crucial in expanding our understanding of the driving of the SAO, including the importance of meridional advection and breaking planetary waves in driving the easterly phase of the SAO. Simulating the westerly phase of the SAO was a challenging problem from the early years. An observational analysis by Hirota (1978) indicated the role of high-speed Kelvin waves in driving the SAO westerlies, and incorporating the Kelvin wave driving in the models led to improvements in the simulation of the SAO westerlies (e.g. Dunkerton, (1979); Gray and Pyle (1986)). Hitchman and Leovy (1988) quantified the contribution of Kelvin waves to the zonal-mean momentum budget and suggested that gravity waves may also contribute to the driving of the SAO westerly phase. Modelling studies like Hamilton and Mahlman (1988) and Jackson and Gray (1994) confirmed that including parametrized gravity wave drag further improved the representation of SAO westerly phases in models. In present-day climate models, parametrized gravity waves are undoubtably the primary driver of the SAO westerly phase (Jaison et al., 2024b; Smith et al., 2023). However, multi-model analyses continue to report that a significant easterly bias remains in the modelled SAO (Amodei et al., 2001; Smith et al., 2022).

The Quasi-Biennial Oscillation initiative (QBOi) is an international project (Anstey et al., 2020; Butchart et al., 2018) sponsored by the Atmosphere Processes And their Role in Climate (APARC) programme. It aims to assess and improve the QBO representation in global climate models. As part of QBOi phase 1, Smith et al. (2022) compared the modelled SAO in 11 stratosphere-resolving climate models. While their study highlighted that the models were able to simulate many important properties of SAO, it was noted that nearly all the models exhibit an easterly bias in the zonal-mean zonal wind

https://doi.org/10.5194/egusphere-2026-4135
Preprint. Discussion started: 22 July 2026

SAO. Similar to previous studies (e.g., Burrage et al., 1996; Dunkerton and Delisi, 1997; Garcia et al., 1997; Garcia and Sassi, 1999; Peña-Ortiz et al., 2010; Ray et al., 1998; Richter and Garcia, 2006), all the models demonstrated a strong dependence of the SAO winds on the underlying QBO phases. Vertically propagating waves reaching the SAO altitudes also exhibited this dependence on the QBO phase. This suggests that if the models have a wind bias at QBO levels then it is likely to result in a corresponding wind bias at the SAO levels. It is also known that most models have an easterly phase QBO that is generally too weak and thus exhibits a westerly time mean wind bias throughout the depth of the QBO (Bushell et al., 2022; Garfinkel et al., 2022; Rao et al., 2020).

As part of QBOi phase 2 (Anstey et al., 2026), a further set of climate model simulations were performed, including a free-running control simulation and a nudged simulation in which the equatorial zonal mean zonal winds are nudged towards reanalysis data (see section 2 for details of how this nudging was performed). In an initial study, Jaison et al. (2024b) examined the impact of this bias-corrected QBO on the SAO in a single model, HadGEM3. They concluded that the SAO winds changed by nearly 25% when the QBO was corrected, with a decreased strength of SAO easterlies and an increased strength and duration of SAO westerlies, though a significant bias remained. Changes in gravity wave driving at SAO altitudes, in response to the corrected QBO, were identified as the major contributor to these changes in the SAO. In the present study we extend the analysis of Jaison et al. (2024b) by performing the corresponding analysis using data from state-of-the-art climate models that participated in QBOi phase 2. A comparison of how these models respond to corrections in zonal-mean zonal wind QBO biases is examined and the robustness of results presented in Jaison et al. (2024b) is therefore assessed.

2 Data and Methods

The study uses Modern-Era Retrospective Analysis for Research and Applications, Version 2 (MERRA-2) reanalysis data for comparing SAO characteristics with QBOi phase 2 models. The MERRA-2 reanalysis dataset (Gelaro et al., 2017) is provided by the National Aeronautics and Space Administration (NASA) Goddard Institute for Space Studies (GISS) and is available from 1980. All results shown in the paper employ MERRA-2 data for the time period 1980-2021. This global reanalysis dataset has a horizontal resolution of 0.5° latitude x 0.625° longitude and has 72 hybrid eta model levels in the vertical extending from surface to 0.01hPa. The climatological SAO in MERRA-2 zonal-mean zonal wind is shown in figure 1 (see also Jaison et al. (2024b)). Earlier studies have noted that the MERRA-2 dataset has a reasonable SAO representation in comparison with observations (Ern et al., 2021), possibly due to assimilation of Microwave Limb Sounder (MLS) temperature data at altitudes of 5 hPa and above, along with a non-orographic gravity wave parameterization tuned to better represent equatorial stratospheric variability (Molod et al., 2015). However, artificial damping (Rayleigh friction) is applied to horizontal winds at altitudes above 0.24 hPa in the assimilation model. Thus, the winds are most likely weaker and less reliable at these higher altitudes. There are also differences in the SAO between available observations (Kawatani et al.,

https://doi.org/10.5194/egusphere-2026-4135
Preprint. Discussion started: 22 July 2026

2020), but these discrepancies are relatively small compared with the biases in the modelled SAO. We also note that the first decade of the MERRA-2 zonal mean zonal wind data exhibits spurious semiannual variations at 10 hPa, as there is an enhanced downward propagation of the SAO westerlies during QBO easterly phases (Kawatani et al., 2016). Given these caveats, in this study, the MERRA-2 analysis focuses primarily on winds near ~1 hPa, where the SAO signal is stronger and more reliable.

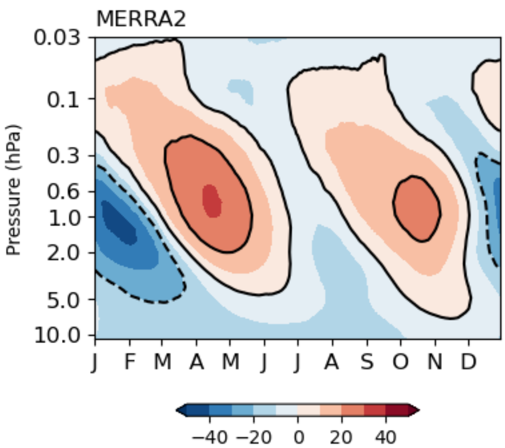

Figure 1: Height time-series of climatological daily-mean, zonal-mean zonal wind (ms−1) averaged over 15°N to 15°S derived using MERRA-2 data for the period 1980-2021. Contours of -10, 0, 10 ms^{-1} are overlaid, with dashed contours denoting negative values.

The model datasets analyzed in this study are from QBOi phase 2, which aims to assess how QBO teleconnections perform when biases in the simulated QBO are removed (Anstey et al., 2026). Data from twelve models are available, each comprising simulations extending from January 1979 to December 2020. We note that some of the models have been updated from the versions that participated in QBOi Phase 1, and the simulations now cover a 42-year period compared to the 30-year period used in the previous phase.

In this study 10 of the 12 participating models are analyzed, HadGEM3 GA7.1, MIROC6.1 (p1), MIROC6.1 (p2), LMDz6, CAS-ESM, E3SM2 (Golaz et al., 2022), GFDL-ESM4, MRI-ESM2.0, EC-Earth3 and CESM2(CAM6). One model (BCC-CSM2-MR) was excluded due to a lower model lid placed within the SAO altitude, and two further models excluded due to unavailability of data. The dataset is particularly suitable for analyzing SAO representation, as most models in the project have their upper boundaries in the mesosphere or thermosphere (Anstey et al. (2026), see their table 3). However, some models employ sponge layers that extend into the SAO region. For example, EC-Earth3 applies Rayleigh friction at the upper model levels, while E3SM2 applies a ∇^2 Laplacian operator to all prognostic variables in the top six model layers.

Two experiments from QBOi phase 2 are analyzed in this study and are referred to as the ‘Control’ and ‘Nudged’ experiments. Most models have three ensemble members available for each experiment, except EC-Earth3 with only one

https://doi.org/10.5194/egusphere-2026-4135
Preprint. Discussion started: 22 July 2026

ensemble member each for the Control and Nudged experiments, and LMDz6 with only one ensemble member for the Control experiment. In the Control experiment the modelled QBO was allowed to evolve freely and in the Nudged experiment the equatorial stratospheric zonal-mean zonal winds were nudged towards European Centre for Medium-Range Weather Forecasts (ECMWF) Reanalysis v5 (ERA5; Hersbach et al., 2020) zonal-mean field in the height region of the QBO, with a nudging time scale of 5 days, which is thought to be enough to constrain the slowly evolving QBO winds. The nudging methodology followed the Stratospheric Nudging And Predictable Surface Impacts (SNAPSI) protocol (Hitchcock et al., 2022), although the nudged regions and timescale differ from that used by the SNAPSI programme. The nudging was fully applied between 10-70 hPa with gradual tapering to zero by 100 hPa and 5hPa, and between 10°S-10°N, with tapering to zero by 20° latitude. This ensured that the nudging was applied only to the QBO region and the zonal winds in the SAO region were allowed to evolve freely. The details of the nudging methodology used in the QBOi phase 2 are outlined in Anstey et al. (2026). While nudging only the zonal-mean zonal wind was requested in the protocol, in some models (E3SM2, ESM4 and EC-Earth3) this was not feasible and full-field nudging (i.e. nudging towards zonally-varying local winds rather than the zonal-mean) was implemented.

CMIP6 external forcings are generally used by most models. For the ocean boundary, AMIP boundary conditions for observed SST and sea-ice from input4mip (https:// aims2.llnl.gov/search/input4MIPs/) were prescribed. The models analyed in this study also include CMIP6 forcings from time-evolving volcanic aerosols (except in LMDz6), 11-year solar cycle (except in LMDz6) and trace gas concentrations. Some participating models have interactive ozone, while the observed climatological or transient ozone is specified in other models. In the QBOi 2 protocol it was proposed to use the observed monthly climatological ozone field in models with non-interactive chemistry, rather than a fully transient ozone field since the latter will contain a QBO signal that is inconsistent with the spontaneous QBO generation in the Control experiments (Butchart et al., 2023).

As the current climate models are not able to produce realistic tropical stratospheric oscillations with only resolved waves, physical parametrization of gravity waves is unavoidable. The gravity wave parametrization usually involves representation of wave generation, propagation and dissipation by filtering at critical levels and wave saturation. All the models analysed in this study have a parametrized non-orographic GW. MIROC6.1, ESM4, MRI and EC-Earth3 have a fixed gravity wave source in the parametrization. Other models, instead of using a fixed wave source, parametrize the source of non-orographic gravity waves by linking to convection or frontal systems, as these are the primary sources of non-orographic gravity waves in our atmosphere. The details for non-orographic gravity wave parametrization can be found in (Anstey et al., (2026); see their table 4).

To compare the SAO among the models, the semi-annual amplitude and phase are calculated by filtering out the other frequencies. This analysis was carried out using a Fourier transform. In the time series data (of length T), Fourier analysis

https://doi.org/10.5194/egusphere-2026-4135
Preprint. Discussion started: 22 July 2026

was performed to obtain the Fourier coefficients of the n^{th} harmonic, a(n) and b(n), corresponding to the six-month variability (hence T/n = 6 months). The amplitude is then calculated as $SAO_{\text{amplitude}} = \sqrt{a(n)^2+b(n)^2}$. The phase was calculated as the inverse tangent of (b(n))/(a(n)), with the resulting value in radians. To present the phase more intuitively, the value in radians was converted into a corresponding number of days (by scaling with (1/2π) (T/n)).

Statistical properties of the SAO in the analysed models are depicted using a 'violin plot' showing the kernel density distribution of the frequency of occurrence (number of months) of wind strength. Kernel density estimation smooths the data (monthly data of tropical-mean zonal wind strengths at a specific altitude) with a Gaussian kernel, producing a continuous density estimate. While smoothening of the data may obscure fine-scale features, the method helps to easily identify the overall distribution shape, and combined with important statistics such as mean, median and skew, provides a convenient way to compare Control and Nudged experiment zonal winds.

To examine the impact of the time-evolving QBO on the SAO in each model, a 1000-day composite time-series of zonal-mean zonal winds is calculated, in which the QBO easterly (QBOE) to QBO westerly (QBOW) transitions are aligned. The raw monthly-mean zonal-mean zonal-wind data averaged over 15° S to 15° N at 10hPa is used to identify the months in which QBO transition from westerly to easterly phase. To avoid counting instances where SAO westerlies reach 10hPa without an accompanying QBO westerly phase, it is ensured that the zonal-wind average for the next 4 months remains westerly. Depending on whether the transition aligns close to NH or SH autumn, a 1000-day window is selected, starting either from March 1st or September 1st, and the composite is calculated. This ensures that day zero of the composite roughly aligns with an SAO westerly (SAOW) phase, which occurs near the equinox. And a 1000-day window is chosen to capture the full cycle of the QBO, as QBO period can extend up to 34 months (Baldwin et al., 2001). The method is similar to the one used to produce the HadGEM3 composite presented in Jaison et al. (2024b) (see their figure 3). It is important to note that this composite shows an average over many QBO cycles and can be affected by the cycle-to-cycle variability in each QBO phase. Nevertheless, this approach allows the visualization of the evolution of the SAO cycles as the westerly phase of the QBO descends.

A standard QBO composite separating QBO westerly and easterly months is used, calculated from the monthly-mean zonal-wind data. The QBOE and QBOW months are identified as months in which zonal-mean zonal winds averaged over 15° S to 15° N are easterly or westerly respectively at 10hPa. This approach differs from Jaison et al. (2024b) who used 50hPa as the reference level. Calculations show that in the Nudged experiments (where the 50hPa winds are nearly identical to the ERA5 reanalysis), the ratio of QBOE to QBOW months at 50 hPa is around 1.5. In contrast, all models except HadGEM3 and MRI have ratios higher than 3.5 in their Control experiments, reaching up to 6.5 in LMDz6. Therefore, 50 hPa does not effectively distinguish between QBOE and QBOW phases in most models. The 10 hPa level provides a clearer separation between the QBO phases. At this level, the ratio between QBOE and QBOW months in the Nudged experiments is about

https://doi.org/10.5194/egusphere-2026-4135
Preprint. Discussion started: 22 July 2026

2.5, and in the Control experiments it ranges from 1 to 3.5, aligning more closely with the Nudged results. Thus, the 10 hPa reference level is used for the analysis in this study.

Processes driving the SAO are analyzed using the transformed Eulerian momentum (TEM) equation (Andrews et al., 1987). Acceleration of zonal-mean zonal wind can be written as:

$$\frac{\partial \bar{u}}{\partial t} = -\bar{v}^{*}\left[\frac{1}{a\cos\phi}\frac{\partial(\bar{u}\cos\phi)}{\partial\phi} - f\right] - \bar{w}^{*}\frac{\partial \bar{u}}{\partial z} + \frac{1}{\rho_0 a\cos\phi}\nabla\cdot F + \bar{X} \qquad (1)$$

Where,

$$\bar{v}^{*} = \bar{v} - \frac{1}{\rho_0}\left(\frac{\rho_0\,\overline{v'\theta'}}{\bar{\theta}_z}\right)_z$$

$$\bar{w}^{*} = \bar{w} + \frac{1}{a\cos\phi}\left(\frac{\cos\phi\,\overline{v'\theta'}}{\bar{\theta}_z}\right)_\phi$$

$$\nabla\cdot F = \frac{1}{a\cos\phi}\frac{\partial}{\partial\phi}\left(F^{(\phi)}\cos\phi\right) + \frac{\partial F^{(z)}}{\partial z}$$

and

$$F^{(\phi)} = \rho_0 a\cos\phi\left(\bar{u}_z\frac{\overline{v'\theta'}}{\bar{\theta}_z} - \overline{u'v'}\right)$$

$$F^{(z)} = \rho_0 a\cos\phi\left(\left[f - \frac{1}{a\cos\phi}\frac{\partial(\bar{u}\cos\phi)}{\partial\phi}\right]\frac{\overline{v'\theta'}}{\bar{\theta}_z} - \overline{w'u'}\right)$$

u, v, w and θ represent the zonal wind, meridional wind, vertical wind and potential temperature. The overbar denotes a zonal mean quantity, and the prime denotes departure from the zonal mean. The acceleration of zonal-mean zonal wind is explained by four distinct forcing components in the TEM formulation (Jaison et al., 2024a) The first term on the right-hand side of equation (1) accounts for the contribution of meridional advection, which primarily consists of easterly winds advected by the BDC from summer to winter hemisphere in the context of SAO. Vertical advection by BDC or due to local wave-driven circulation is represented in the second term on RHS of equation (1). The third term is the Eliassen-Palm (E-P)

https://doi.org/10.5194/egusphere-2026-4135
Preprint. Discussion started: 22 July 2026

flux divergence, which indicates the resolved wave forcing and the remaining sub-grid scale processes are part of the fourth term X. In models, X mainly consists of the parameterized gravity wave drag (GWD) and numerical diffusion.

The QBOi phase 2 datasets are provided on specified pressure levels. The zonal-mean diagnostics are available at daily and monthly frequency, with a top available altitude of 0.4 hPa for all models, except HadGEM3 and EC-Earth3 which provide data at higher altitudes. Daily and monthly data of zonal wind and TEM diagnostics are used in this study. The TEM diagnostics are available as direct model outputs, derived from 6-hourly instantaneous samples, and stored as daily and monthly means. CESM2 (CAM6) TEM diagnostics data were not available at the time of this study and only the monthly 3D zonal wind values were provided up to the SAO altitudes. Hence, the CESM2 data is used only in the analysis of the zonal wind changes. The average of all available ensemble members is presented in the results unless otherwise stated. When a comparison between two data sets is presented, a Student's t test is used to calculate if the distributions are significantly different at a particular p-level (5%, or as otherwise stated).

3 Results

3.1 SAO characteristics in QBOi phase 2 models

To gain an understanding of how the QBOi phase 2 models perform in generating the SAO, and how the model performance changes when biases in the zonal-mean zonal wind QBO are corrected, the climatology of zonal-mean zonal wind from 100hPa to 0.4hPa (or the top model level where data is available) averaged over 15°S to 15°N, is examined in Figures 2 and 3. Jaison et al (2024) provided a detailed examination of the SAO in the HadGEM3 model and its response to bias alleviation in QBO. Building on that, for ease of comparison, the models presented here are divided into two groups. The first group, shown in Figure 2, includes models whose SAO climatology of zonal-mean zonal wind and response patterns is similar to that of the HADGEM3 model. This classification is primarily based on comparable SAO amplitude and phase in the control simulations of these models, as discussed in detail later (figure 4b). The second group, shown in figure 3, displays distinctly different characteristics compared to HadGEM3 and are discussed further below. Hereon, the first group of models will be addressed as the 'Similar group' of models and second group as the 'Distinct group'.

The Similar group, shown in Figure 2, is comprised of HadGEM3, two versions of MIROC6.1, LMDz6 and CESM2 (CAM6). Figures 2a,d,g,j and m, showing the Control experiments, indicate that across all these models, from 2hPa to the highest plotted altitude, a reasonable representation of the SAO is evident. The easterly phase occurs during solstices and appears over a range of altitudes at the same time (except in LMDz6) and the westerly phase occurs during equinoxes and descends with time. An annual cycle is also observed in the easterly phase for all models, where the SAO easterly (SAOE) phase in NH winter is stronger than the one during SH winter. The NH winter SAOE peak occurs mostly around 1 hPa, while the altitude of the peak of the SH winter SAOE varies among models. A notable characteristic across the Similar group

https://doi.org/10.5194/egusphere-2026-4135
Preprint. Discussion started: 22 July 2026

models is that either the second easterly phase of the SAO or the westerly phase reaches its peak magnitude at 0.4 hPa or possibly at a higher altitude, although the higher altitudes cannot be verified due to data availability limitations. Although the
275 SAOW phase magnitude is weaker and the easterly phase stronger than that of MERRA-2 SAO (see figure 1), the models in the Similar group still capture the major characteristics of the SAO.

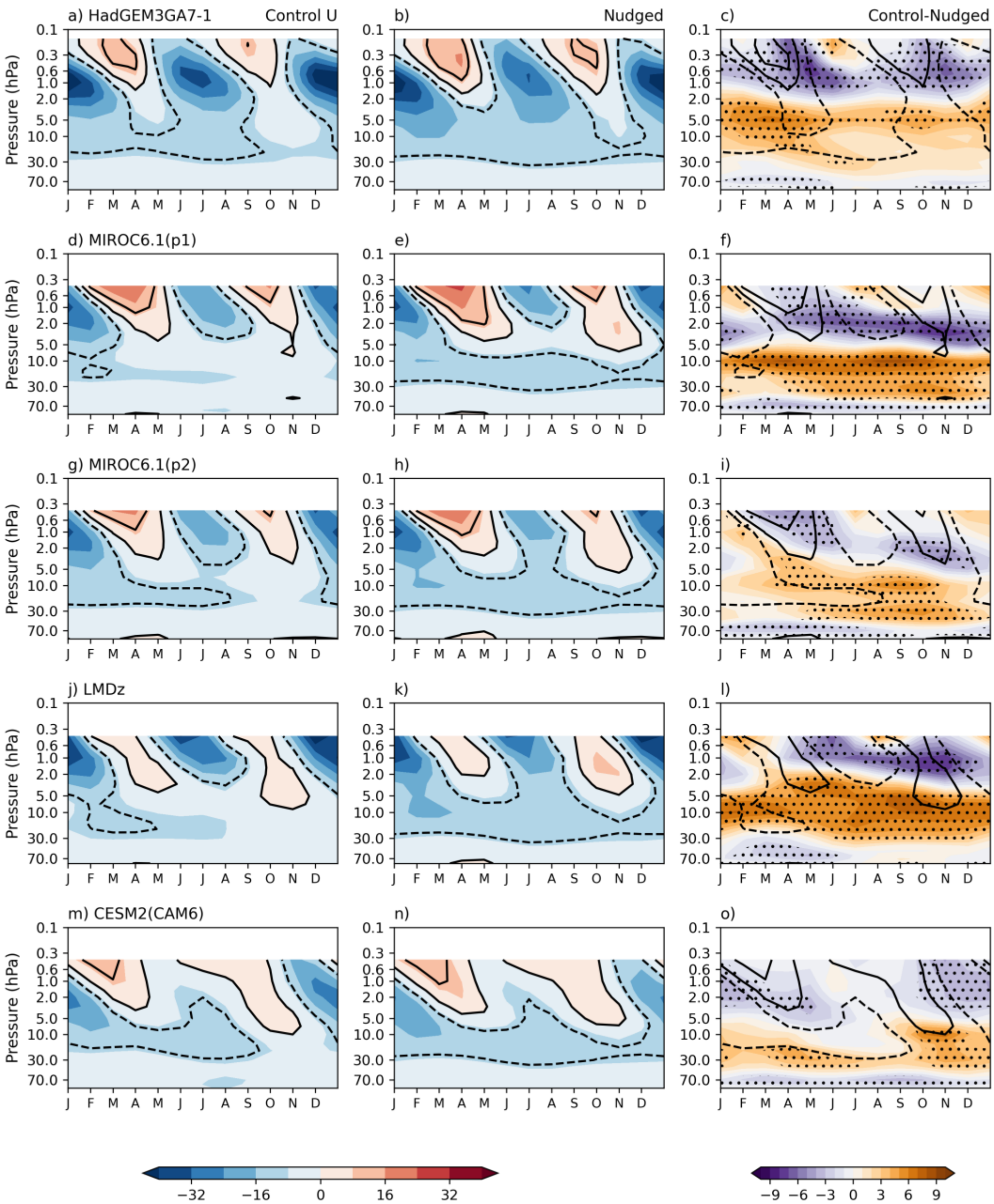

Figure 2: Daily mean climatology of zonal-mean zonal wind (ms−1) averaged over 15°Nto 15°S for Control ensemble-mean, Nudged ensemble-mean and Control minus Nudged differences respectively in (a-c) HadGEM3, (d-f) MIROC6.1(p1), (g-i)

https://doi.org/10.5194/egusphere-2026-4135
Preprint. Discussion started: 22 July 2026

MIROC6.1(p2), (j-l) LMDz6 and (m-o) CESM2(CAM6). Contours of -10, 0, 10 ms^{-1} are overlaid, with dashed contours denoting negative values. Overlaid in c, f, i, l and o are the wind contours from the Control ensemble-mean at -10, 0 and 10 ms^{-1}. Stippling denotes 95% confidence interval.

The Similar group models exhibit similar changes in the SAO in response to the QBO bias correction. From Figure 2b,e,h,k and n, the models' SAOW has generally increased in magnitude and/or descends farther down in altitude, in response to the QBO bias reduction. The SAOE, especially the one during the SH winter, has reduced in magnitude around 1 hPa (although in CESM2 (CAM6), the NH winter changes are prominent). These features indicate a reduction in the easterly bias of SAO in these models.

Panels c,f,i,l,o which display the differences between Control and Nudged experiments for the models in the Similar group, reveal that the magnitude of QBO wind changes due to nudging in the QBO altitudes (from 10 hPa to 100 hPa) are roughly similar across all the models shown. This similarity is also observed at the SAO altitudes, where a similar magnitude change in winds is evident. The time of the year at which the SAO differences peak matches with that of the QBO corrections in most models.

As noted in previous studies, the models generally display a westerly bias at the QBO altitudes (Anstey et al., 2026; Bushell et al., 2022). This bias is largely corrected in the Nudged experiments, as evidenced by the positive values in the difference plots. The negative values dominating the upper stratosphere in the difference plot imply that winds became more westerly in the Nudged experiments, consistent with an improved SAO representation. The comparable biases in QBO winds and the similar vertical profiles of SAO winds across the models may explain why members of the Similar group have similar SAO responses to the QBO nudging.

Figure 3 illustrates the SAO in the zonal-mean zonal wind from the Control and Nudged experiments of the Distinct group of models. While E3SM2 and MRI display alternating easterly and westerly phases of the SAO clearly, the other three models, CAS-ESM, ESM4 and EC Earth3 struggle to replicate SAO variability around 1 hPa. In the latter models, although the easterly phase of the SAO is reasonably represented, the westerly phase, particularly the second cycle of SAO westerlies (occurring during September to November), is nearly absent in these models at 1hPa. Even within E3SM2 and MRI, notable differences are evident compared to reanalysis: E3SM2 lacks annual cycle variability (in which the easterly winds in the second half of the year are stronger than in the first half), and MRI exhibits very weak westerlies (less than 8 ms^{-1}). The altitude of peak SAO easterlies or westerlies in the Distinct group models occurs below 1hPa, which is different from the Similar group models. Except for MRI, all models in the Distinct group struggle to produce the major SAO characteristics.

https://doi.org/10.5194/egusphere-2026-4135
Preprint. Discussion started: 22 July 2026

Based on the response to the nudging, the Distinct group models can be further classified into subgroups. CAS-ESM, E3SM2 and ESM4 can be categorized together. All three models exhibit very strong changes in the SAO winds due to the QBO nudging, shifting towards westerly in most regions, with differences exceeding 10 ms^{-1} for most of the year (as shown in Figure 3 c, f, i difference plot). This could be the result of drastic changes in the QBO from nudging in these models in comparison to others. CAS-ESM and ESM4 also exhibit stronger westerly QBO biases in their control simulations than all of the other models analysed here (Figure S1; also see figure 4a in Anstey et al., (2026)) While the strong changes in QBO due to nudging is immediately visible for CAS-ESM and ESM4 (figure 3c, i), E3SM2 changes are less apparent. Since E3SM2 lacks strong internally generated QBO variability (see Figure S1), introducing nudging significantly alters the winds at QBO altitudes, although the overall climatology changes are less. Figure S1, which shows time evolution of zonal-mean zonal wind averaged over 15°N to 15°S for individual models , also suggests that nudging in CAS-ESM is unsatisfactory as the QBO winds continue to exhibit a westerly bias (also see figure 4a in Anstey et al., (2026)).

The E3SM2 Nudged experiments show stronger SAOW and weaker SAOE, consistent with an improved SAO representation, however, the model still fails to have a proper annual cycle. Even with strong changes in SAO altitudes, the CAS-ESM and ESM4 SAO characteristics have not necessarily improved. ESM4 is particularly intriguing, as it appears to have no phase separation at SAO altitudes, showing only westerly winds. Among the models analyzed in this study, CAS-ESM, E3SM2, and ESM4 have the lowest vertical resolution, with 69, 72, and 49 levels, respectively. Although E3SM2 has 72 levels, its model lid is at 0.1 hPa, placing it within SAO altitudes. The drastic changes in SAO observed in these models in the Nudged experiments could therefore be attributed to factors such as lower vertical resolution, substantial alterations in QBO winds, and the SAO peak occurring below 1 hPa.

The final two models in the Distinct group, MRI and EC-Earth3, show the smallest response at SAO altitudes to the nudging of the QBO. From figure 3l, MRI evidently has the smallest changes at QBO altitudes. This lack of change at the lower altitudes could therefore explain the little to no changes in the SAO. On the other hand, figure 3o suggests that nudging in EC-Earth3 leads to considerable changes in the model QBO winds, comparable in magnitude to the QBO changes in the Similar group models. The free running EC-Earth3 model is already known to show poor SAO representation (see figure 3m and (Döscher et al., 2022). Serva et al. (2024) explored the momentum budget of the SAO and suggested that excessive Rayleigh friction applied at the upper model levels in EC-Earth3 could explain the lack of SAO westerlies around 1 hPa. Thus, even when the QBO in the model is corrected, it appears that due to the Rayleigh drag in the upper stratosphere, the SAO is unable to change significantly. Because of these strong non-physical effects in the upper stratosphere of EC-Earth 3 and marginal changes in SAO, the model is excluded from further analysis. Note that, except for MRI and EC-Earth3, all other models show a maximum of at least 3 ms^{-1} or greater changes at SAO altitudes. With an understanding of the general SAO characteristics in the presented models, the next section will focus on analyzing the multi-model mean behaviours.

https://doi.org/10.5194/egusphere-2026-4135
Preprint. Discussion started: 22 July 2026

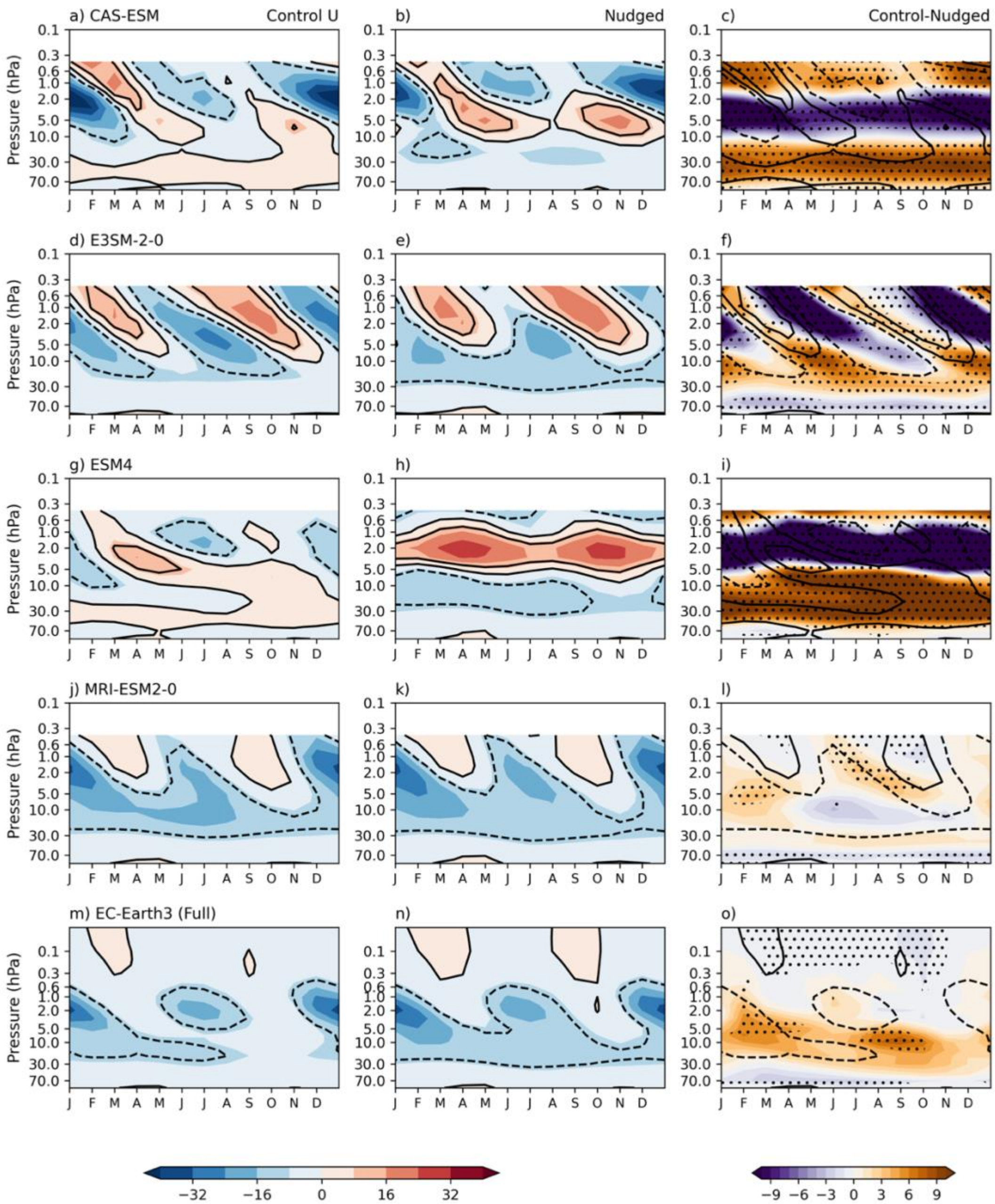

Figure 3: Daily mean climatology of zonal-mean zonal wind (ms−1) averaged over 15°N to 15°S for Control ensemble-mean, Nudged ensemble-mean and Control minus Nudged differences respectively in (a-c) CAS-ESM, (d-f) E3SM2, (g-i) EMS4 , (j-l) MRI and (m-o) EC-Earth3. Contours of -10, 0, 10 ms^{-1} are overlaid, with dashed contours denoting negative values. Overlaid in c, f, i, l and o are the wind contours from the Control ensemble-mean at -10, 0 and 10 ms^{-1}. Stippling denotes 95% confidence interval.

https://doi.org/10.5194/egusphere-2026-4135
Preprint. Discussion started: 22 July 2026

Figure 4a, b, and c display the time-mean, semi-annual amplitude, and phase propagation of the equatorial zonal-mean zonal wind, respectively, across all models in the Control experiments. In the time-mean profile, while most models exhibit mean easterly winds in the QBO region, CAS-ESM and ESM4 show westerly winds, with a difference of nearly 10 ms^{-1} compared to the other models. At SAO altitudes, aside from an overall easterly average, where HadGEM3 shows the largest easterly magnitude, no particularly outstanding patterns are observed. At 1 hPa, all models show an easterly bias when compared to the equivalent MERRA-2 diagnostic.

The semi-annual amplitude provides insight into the location of the peak six-month variability in the models (Figure 4b). Below 10 hPa, this amplitude is minimal as this region is primarily influenced by the QBO. Above 10hPa, the semi-annual variability increases, peaking somewhere above 5 hPa in all the models, before generally decreasing at higher altitudes. The Similar group models (HadGEM3, MIROC 6.1(p1), MIROC 6.1(p2) and LMDz6) show peak SAO amplitude between 1hPa and 0.3 hPa (except for HadGEM3, 0.4hPa is the highest altitude for which model data is available from these models). This magnitude compares well with the SAO amplitude of MERRA-2 (which peaks at 1 hPa). E3SM2 shows a similar magnitude peak, but at a much lower altitude, between 5hPa and 2hPa. The model lid of E3SM2 is at 0.1 hPa, which might explain the lower altitude peak. Among the Distinct group models, all except E3SM2 exhibit peaks between 2 hPa and 1 hPa, with significantly smaller SAO amplitudes, reduced by nearly 10 ms^{-1} in MRI, and ESM4. This is consistent with Figure 3, where these models show much lower wind amplitude compared to the remaining models.

The phase, defined as the timing of first maximum of the semi-annual variability (see section 2 for details of calculation), varies from early-March to mid-April (roughly from days 60 to 110) depending on model. The Similar group models with higher altitude SAO peak have faster downward phase propagation, which is more similar to MERRA-2. Based on both SAO amplitude peak and phase, the Similar group models are closer to MERRA-2 in replicating SAO characteristics, although they nevertheless still have an easterly wind bias in terms of magnitude.

Figure 4 d, e and f illustrate the multi-model ensemble average (MME) of time-mean, semi-annual amplitude, and phase propagation of the zonal-mean zonal wind of the eight models discussed. The blue line represents the average of the Control experiments, as seen in Figure 4a-c, while the red line indicates the properties of the Nudged experiments. The shading shows the standard deviation of the variable across the models. The time-mean profile (Figure 4d) clearly suggests that nudging has caused the QBO winds (from 70 hPa to 5 hPa) to become more easterly, while the SAO winds have shifted to more westerly. This adjustment reduces the westerly bias in the QBO within the models which, in turn, helps to reduce the easterly bias of the SAO. The amplitude and phase (3e,f) show little to no change, with the phase slightly shifting to later days but this is statistically insignificant around 1hPa.

https://doi.org/10.5194/egusphere-2026-4135
Preprint. Discussion started: 22 July 2026

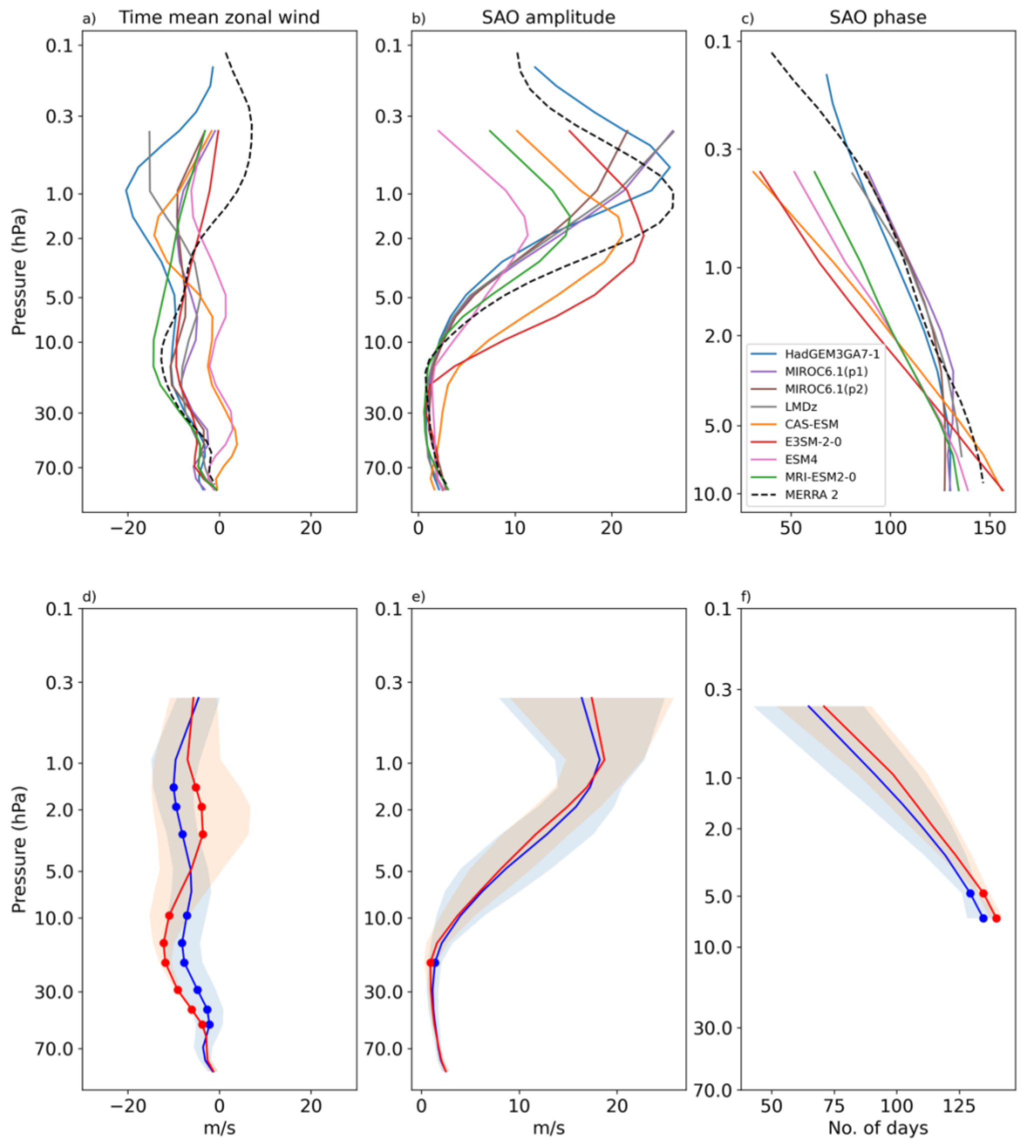

Figure 4: Height profiles of (a) the multi-year climatology of equatorial zonal-mean zonal wind, (b) amplitude of the semi-annual component and (c) phase of the semi-annual component derived from the Control experiments of 8 different models. Units are ms−1. The multi-model mean (red line) and standard deviation (red shading) are shown in (d-f) along with the corresponding profile from the Nudged experiments (blue line and blue shading). Significantly different data points at 95% confidence interval are marked as blue and red dots in (d-f).

https://doi.org/10.5194/egusphere-2026-4135
Preprint. Discussion started: 22 July 2026

The latitudinal profile of the SAO in the models is explored in Figure 5. The figure presents the latitudinal profile of time-mean and semi-annual amplitude of zonal-mean zonal wind at 1 hPa, where, from Figure 4b, all models showed reasonable SAO amplitude. The Control experiment behaviour is consistent with the QBOi phase 1 models (Smith et al., 2022). In terms of the mean wind, MERRA-2 exhibits a peak at the equator which falls off away from the equator and then slightly increases around 30 degrees in both hemispheres. However, the models show inconsistent behaviour. About half of them display a peak at the equator, while the others show a minimum, and none have the time-mean wind at the equator as westerly as observed in MERRA-2.

The latitudinal profile of the amplitude of the semi-annual harmonic is more consistent across models. All the models except ESM4 show a maximum amplitude south of the equator within 20 degrees. MERRA-2 displays a similar feature as well but with a slightly higher amplitude.

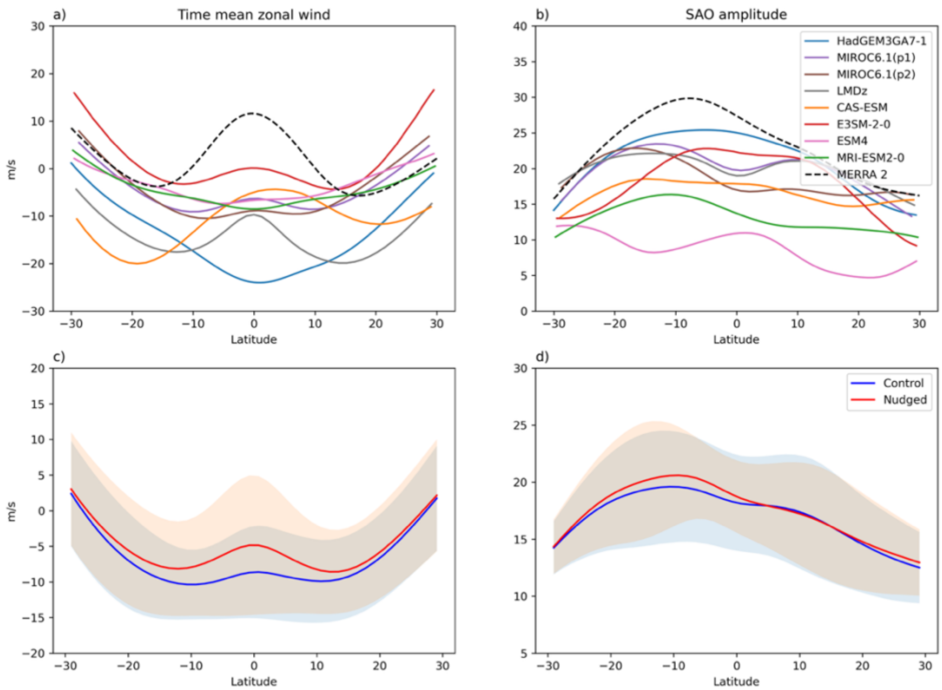

Figure 5: Climatology and amplitude of semi-annual component of zonal-averaged zonal winds as in figure 4 but showing the latitudinal variation at 1 hPa.

Figure 5c,d indicates that the Nudged experiment (red) becomes noticeably more westerly at the equator compared to the Control experiment (blue), shifting closer to the MERRA-2 values. However, the difference between the Control and

https://doi.org/10.5194/egusphere-2026-4135
Preprint. Discussion started: 22 July 2026

Nudged experiments is statistically insignificant and diminishes at higher latitudes, around 20 to 30 degrees. Since nudging is applied between 20°S and 20°N in all models, this latitudinal profile suggests that the QBO's influence on the SAO might be primarily vertical. In the NH, time-mean wind values align with MERRA-2 after 20 degrees. The SAO amplitudes in the Nudged MME are slightly higher in the SH compared to the Control, though the overall changes appear minimal and statistically insignificant.

To further quantify the difference between SAO wind strength in the Control and Nudged experiments, Figure 6 shows the equatorial zonal-mean zonal wind distribution of each model at a specified altitude (determined as described below), presented as the kernel density distribution of the frequency of occurrence (number of months) of wind strengths. The width of a distribution roughly indicates the number of months equatorial winds are at a certain strength, smoothed with kernel density estimate (see section 2 for details). From figure 4 it is evident that the altitude at which the multi-year wind climatology and the semi-annual amplitude peaks varies among models. Thus, instead of selecting a standard pressure level on which to analyze all the models, we have selected a separate altitude for each model, depending on its vertical wind distribution. This was done by calculating the difference of the multi-year zonal-mean equatorial zonal wind climatology (averaged over 15°S to 15°N) between the Control experiments (see figure 4a for Control climatology) and Nudged experiments to identify the altitude above 5 hPa where the difference maximises (see table 1). The change in wind characteristics at the identified altitude for each model is then displayed in figure 6.

In all the models analysed the mean value of the Nudged experiment is consistently more westerly than the Control experiment (although the changes in MRI were found to be insignificant). Table 1 shows that in six of nine models, the mean wind has shifted by a minimum of 4 ms^{-1}. The percentage change in winds (Nudged – Control) with respect to the Control experiment winds in each model, calculated using the mean values from figure 6, is also indicated in table 1. We note that the mean value of the Control experiment wind differs across models, however, using percentage change offers an effective method for comparing the models. The Similar group models show that the winds became more westerly in the Nudged experiment with respect to the Control experiments by a factor of 23% - 57%. The changes in the Distinct group models, on the other hand, are either much higher (two to four times increase) or much lower (6% in MRI).

Not only the mean but also the median has shifted to less negative/more positive values in all the models. Additionally, the skew values in Table 1 are more negative in the Nudged simulations (except in CAM6), indicating a reduction in the distribution of easterly winds and a concentration of values toward the westerly side. The 'violin' plots in figure 6 are consistent with these shifts in skewness, showing that the width of the density distribution has decreased on the easterly end and increased on the westerly end in the Nudged experiments for most models. The analysis suggests that in the Nudged experiments, the number of months in which the winds are westerly has increased and the number of months in which

https://doi.org/10.5194/egusphere-2026-4135
Preprint. Discussion started: 22 July 2026

easterlies occupy the upper stratosphere has decreased. And, in some models, the maximum value of westerly winds at the selected altitude has increased as well.

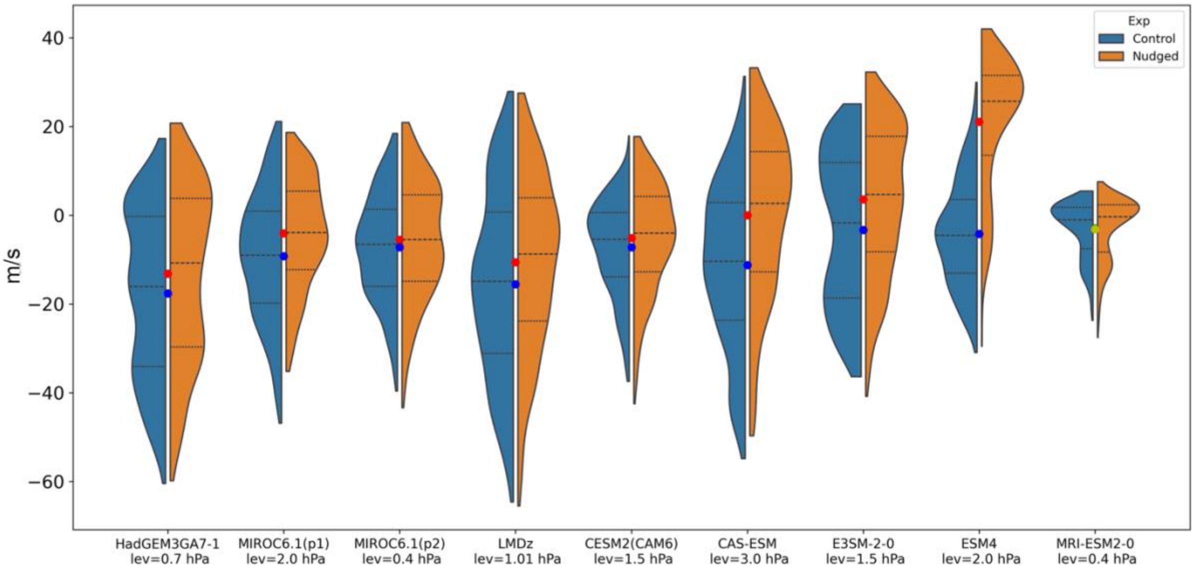

Figure 6: Density distribution of the frequency of occurrence (number of months) of zonal-mean equatorial zonal wind strengths, averaged over 15°S to 15°N, at a selected pressure level for each QBOi model with monthly data from all the available years. For visualization purposes, maximum width is kept the same for all the distributions. The model name and selected pressure level is shown on the x axis label. The pressure level was selected for each model depending on the maximum wind differences between the Control and Nudged experiments (see text). The blue (orange) shading shows the distribution of the Control (Nudged) experiments, with the blue (red) dots showing the mean of the distributions. The dashed lines show the quartiles of the distribution. The difference between the mean of the Control and Nudged distributions is significant for all models except for MRI-ESM2.0 (where the means are shown as green and yellow dots).

Models	Pressure at which maximum wind change occur (hPa)	Difference in mean (Nudged-Control) (ms^{-1})	Percentage change with respect to Control (%)	Control run wind (ms^{-1})	Skew value Control run	Skew value Nudged run
HadGEM3GA7.1	0.7	4.4	24.9	-17.6	-0.18	-0.26
MIROC6.1(p1)	2.0	5.2	56.3	-9.2	-0.18	-0.329
MIROC6.1(p2)	0.4	1.7	23.6	-7.2	-0.146	-0.269
LMDz	1.01	4.95	31.9	-15.5	-0.024	-0.342
CESM2(CAM6)	1.5	2.1	29.1	-7.2	-0.549	-0.465
CAS-ESM	3.0	11.3	100.5	-11.3	-0.283	-0.534
E3SM2	1.5	6.9	208	-3.3	-0.111	-0.358
ESM4	2.0	16.9	403.6	-4.2	0.255	-0.984
MRI	0.4	0.2	6	-3.1	-0.953	-0.984

https://doi.org/10.5194/egusphere-2026-4135
Preprint. Discussion started: 22 July 2026

Table 1: Characteristics of equatorial zonal-mean zonal wind at the SAO altitude where maximum difference between Nudged and Control experiment winds occurs in each model.

3.2 Processes driving the SAO

So far, we have seen that while all the models exhibit an easterly bias in the SAO, nudging the zonal winds towards a more realistic QBO has helped reduce this bias by shifting the SAO winds more eastward in most models. This is particularly the case in the Similar group of models where a noticeable improvement in the SAO characteristics and evolution is evident. In this section, the various forcing terms of the SAO are examined to identify which factors play a major role in modifying the SAO in these models. In Jaison et al. (2024b), GWD was identified as the most changed forcing term at SAO altitudes in HadGEM3. Here, the differences in TEM terms between the Control and Nudged experiments across all models are analyzed to identify the dominant term(s) and investigate the robustness of the result obtained in Jaison et al. (2024b).

Figure 7 illustrates the vertical profile of the difference in each term of the TEM equation between the Control and Nudged experiments for each model (the actual vertical profiles of the Control and Nudged TEM diagnostics are provided in Figure S2). As noted in earlier studies, meridional advection typically contributes to westward forcing, while GWD and vertical advection primarily generate eastward forcing. Additionally, the resolved wave components average out as a source of westward forcing (Figure S2). The remaining forcing (the difference between rate of change of zonal-mean zonal wind and the sum of advection and wave forcings) is also included in Figure S2.We note that in all the models this remaining term is weaker than most of the other TEM forcing terms at SAO altitudes.

In Figure 7, the broad yellow line represents the difference between the zonal-mean zonal wind in the Control and Nudged experiments. The wind profiles for all models, except for MRI, align with the MME average characteristics outlined in Figure 4d. Specifically, positive differences in the QBO region indicate that the nudging effectively alleviates the westerly QBO bias in these models, and this results in a corresponding eastward shift (negative values) at SAO altitudes.

In all the models GWD (red line in Figure 7) is the predominant factor contributing to the difference between Control and Nudged experiments at SAO altitudes. Changes in GWD are closely aligned with changes in the wind profile, although the peak GWD change occurs at slightly lower altitudes. In some models, vertical advection also shows changes of a similar magnitude but in the opposite direction, which could be partly due to an induced circulation from increased eastward GWD forcing, and partly due to vertical gradient of zonal mean zonal wind. At higher altitudes, the opposing changes in vertical advection diminish first, while GWD changes persist, thus the peak wind changes occur slightly above the peak GWD changes.

https://doi.org/10.5194/egusphere-2026-4135
Preprint. Discussion started: 22 July 2026

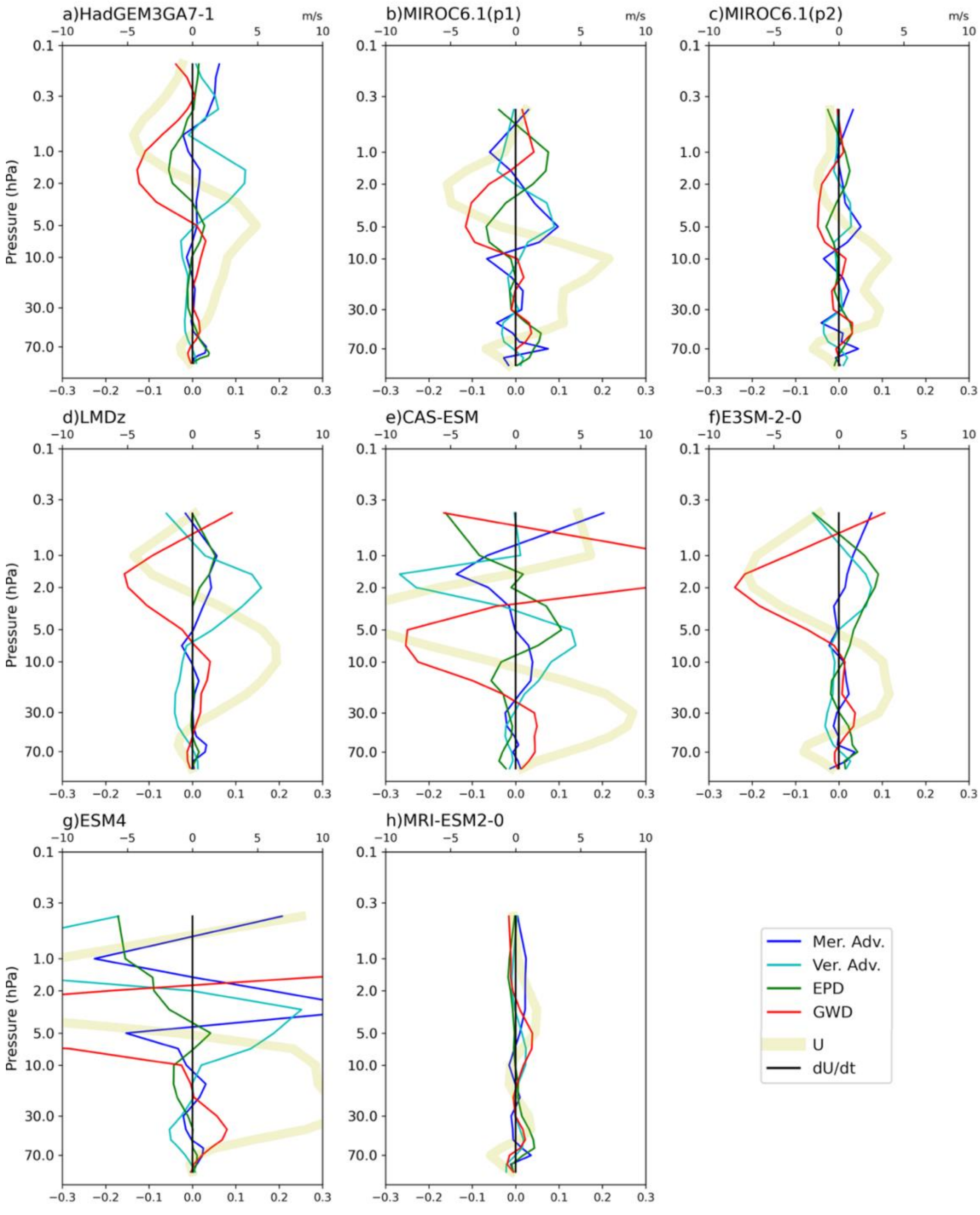

485 **Figure 7: Multi-year annual mean of TEM forcing terms (see legend) and zonal-mean zonal winds (thick yellow line) averaged over 15°S-15°N for Control minus Nudged differences for 8 models, indicated by labels. Units of TEM forcing terms are ms^{-1}day^{-1} (lower axis) and zonal-mean zonal wind is ms−1 (upper axis). In the Similar group models, resolved waves also exhibit increased**

https://doi.org/10.5194/egusphere-2026-4135
Preprint. Discussion started: 22 July 2026

eastward forcing, similar to GWD, but at lower SAO altitudes. In MIROC, meridional advection also contributes to increasing the westward forcing, working alongside vertical advection to counteract the effects of GWD and resolved waves.

The Distinct group of models with the most significant changes in SAO winds, CAS-ESM, ESM4, and E3SM2, are also associated with the largest changes in forcing terms. While GWD remains the dominant term, other terms exhibit substantial changes as well. In these models, the GWD changes in the QBO region, particularly between 100 and 30 hPa, are notably large as well. This excess GWD, which propagates to SAO altitudes, can lead to considerable wind changes due to the lower air density at those heights. MRI, as expected, shows the least changes in forcing terms. In summary, the comparison of TEM diagnostics in all the models suggests that the result from HadGEM3, indicating that GWD is the TEM forcing term affected the most by the nudging, is robust across all the models where a strong change in SAO winds is observed.

3.3 SAO variations over the QBO cycle

To examine the impact of the QBO on the SAO in each model, Figure 8 shows a 1000-day composite time-series of zonally-averaged zonal winds, beginning from March or September immediately before the QBOE to QBOW transitions, so that day zero aligns with an SAO westerly phase (see Section 2 for further details). This allows us to explore how SAO characteristics evolve over multiple cycles as the QBO progresses. The method is identical to the one used to produce the HadGEM3 composite presented in Jaison et al. (2024b) (see their figure 3) except that 10 hPa is used as the reference level to identify when the QBO winds transition instead of the 5 hPa level previously used for HadGEM3. The change to using the 10 hPa level was necessary because in some models the SAO extends further down than 5 hPa.

Figure 8 shows this composite time-series for the multi-model ensemble-mean of the Similar group of models (composites for the individual models are provided in Figure S3). In the Control experiment (figure 8a), as the QBO descends over time the SAOW also descends to lower altitudes. The SAOE is also modulated by the QBO, with the easterly phase magnitude peaking when the QBO westerlies are present between around 5hPa to 10hPa. From the Nudged experiments of these models (figure 8b), it is evident that nudging reduces the magnitude of the QBO westerly winds, occurring during the first 300 days and increases the QBO easterly magnitude. In response, the SAO westerlies propagate further down (see SAO westerlies around days 200 and 400), and the SAO easterlies have reduced in magnitude. This is also evident in the difference plot (figure 8c) which shows strong positive values at QBO altitudes (~5hPa), which further descends over the time window shown. Simultaneously, a similar pattern in SAO winds emerges as negative values, indicating increased SAO westerly winds, decreased SAO easterly winds, or SAO westerlies extending further down in altitude in the Nudged experiments.

The composite time-series of the Distinct group models are not discussed as the QBO nudging resulted in either no change in the SAO or in westerlies dominating the upper stratosphere rather than an improvement in SAO characteristics. Additionally, in the Control experiments of the Distinct group, E3SM2 lacks QBO variability, while CAS-ESM and ESM4

https://doi.org/10.5194/egusphere-2026-4135
Preprint. Discussion started: 22 July 2026

have consistent westerlies at QBO altitudes for most of the period shown (see figure S1 and S3). In addition, results from the CAS-ESM Nudged experiment (figure S3) suggest that the imposed nudging has not been entirely effective, as its QBO is not comparable to that of other models' Nudged experiments.

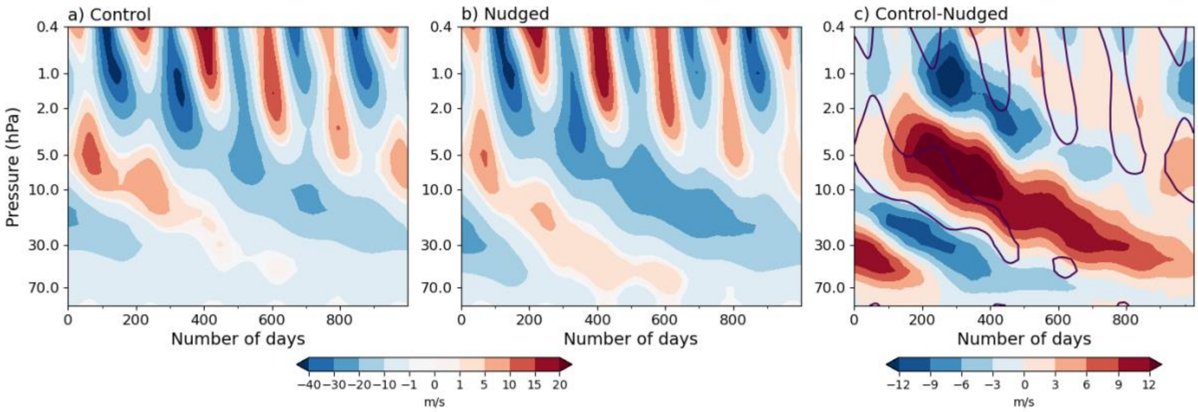

Figure 8: Height time-series composites of zonal-mean zonal wind (ms−1) for the multi-model ensemble mean of the Similar group of models. (a) shows the Control experiment and (b) shows the Nudged experiment. The composite members start from 1st of March or 1st of September whichever is closest to the start of the QBOW phase. The 10hPa reference level is used to identify the start of the QBO westerly phase in the models (see text for more details). Difference between the Control and Nudged experiments are shown in (c) with the time-series composite winds from the Control experiment overlaid as black contours.

In figure 9 the SAO wind dependency on each phase of the QBO is further explored using QBOE and QBOW monthly composites. The months in which the zonal-mean equatorial zonal wind (15°S to 15°N) at 10hPa are classified into QBOE and QBOW, depending on whether the magnitude is negative or positive respectively. As noted in the previous paragraph, CAS-ESM, E3SM, and ESM4 show unreliable QBO characteristics in their Control experiments, either exhibiting excessive westerly winds or lacking QBO variability altogether. Therefore, these models are excluded from the analysis of QBOE and QBOW phases due to their inadequate representation of QBO phase distinctions. In this study, a 10 hPa reference level is used for QBO phase analysis, different from the 50 hPa level used in Jaison et al. (2024b) as some models do not have QBO propagation below 50 hPa in their Control experiments (see section 2 for more details).

Figure 9 a, b shows the QBOE and QBOW composites of zonal-mean zonal wind (solid lines) for the Control experiments of all the models. The SAO winds in the QBOW composite are notably more easterly compared to the QBOE composite. This is expected, as more eastward waves are filtered during the QBOW months and more westward waves propagate to higher altitudes unaffected, resulting in an overall easterly shift in SAO winds.

Figure 9 c, d shows the difference between the Control and Nudged experiment QBO composites during QBOE and QBOW months. These difference plots indicate that above 5 hPa the winds generally become more westerly in the Nudged experiments during the QBOW phase since the Control minus Nudged difference is negative in figure 9d. (We note that

https://doi.org/10.5194/egusphere-2026-4135
Preprint. Discussion started: 22 July 2026

when the QBO winds at 10hPa are westerly, the 50 hPa winds roughly have the opposite sign, and are thus in the QBOE phase. Since 50 hPa was used as reference level in Jaison et al. (2024b), HadGEM3 was noted to improve most during QBOE phase. However, when 10 hPa winds are taken as the reference, HadGEM3, like other Similar group models show maximum improvement in the SAO during the QBOW phase). The models exhibit only minor changes in the SAO during QBOE months, despite the QBO changes being of similar magnitude in both phases.

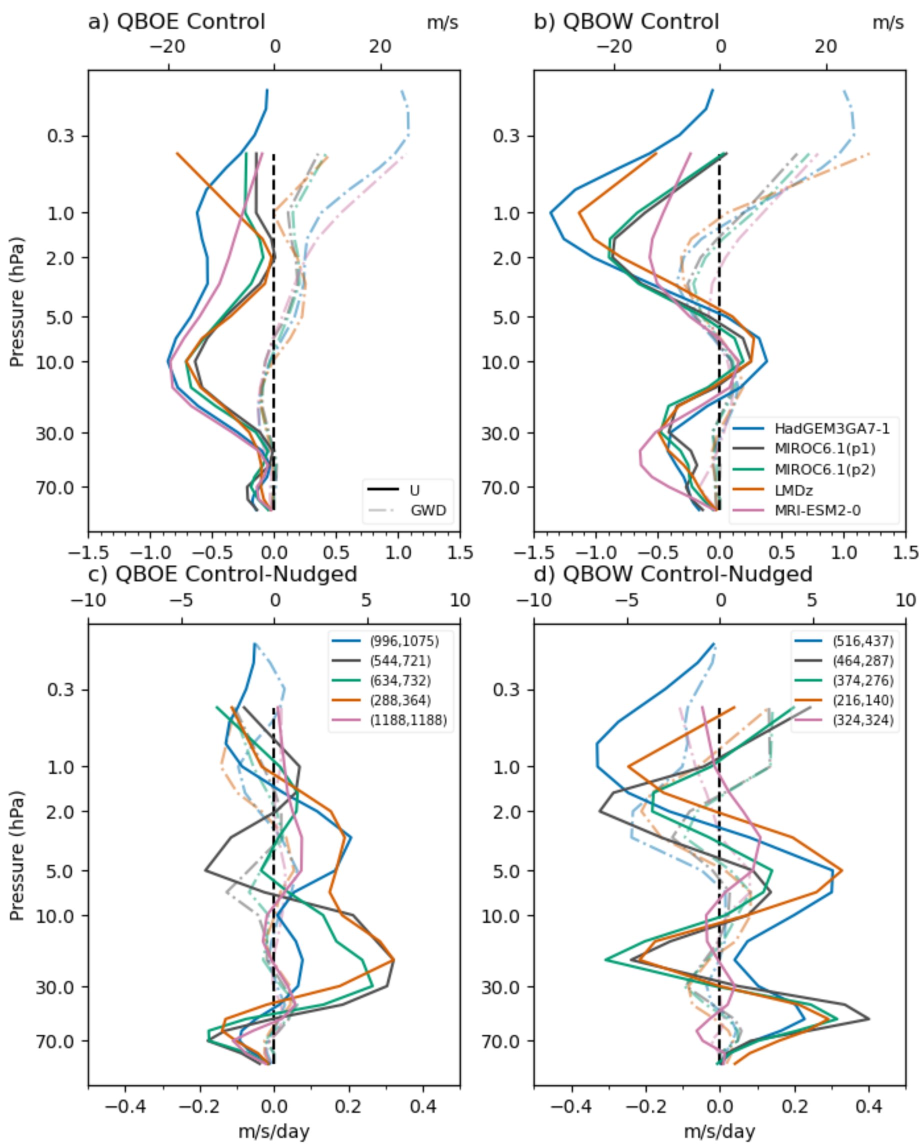

Figure 9: Composite of time-mean zonal mean zonal wind (solid line) and gravity wave drag (dash-dot line) averaged over 15°S-15°N for (a) Control experiment in QBOE months, (b) Control experiment in QBOW months, (c) Control minus Nudged differences during QBOE months, (d) Control minus Nudged differences during QBOW months for 5 models. The numbers in

https://doi.org/10.5194/egusphere-2026-4135
Preprint. Discussion started: 22 July 2026

legend in (c,d) implies number of months in the composite for Control and Nudged experiment respectively. Units of wind is ms^{-1} (upper axis) and gravity wave drag is $ms^{-1}day^{-1}$(lower axis).

All the TEM forcing terms discussed earlier were also examined using the QBO phase composites. The GWD composite is shown as dash-dot lines in figure 9. The Control GWD composite during each QBO phase shows pattern that can be expected from the wind profile shown in figure 9 (solid lines). During the QBOE phase the Control experiment has more eastward GWD forcing between 5 hPa to 1 hPa, while this region is occupied by westward GWD during the QBOW phase. This is consistent with more eastward gravity waves being filtered at critical levels when the QBO winds are westerly, while more westward gravity waves filtered when QBO winds are easterly. Above 1 hPa, GWD is eastward during both QBO phases.

In figure 9c, d, the profile of Control minus Nudged difference for the GWD term closely resembles the zonal-mean zonal wind profile shown. During the QBOW phase (figure 9d), GWD above 5 hPa predominantly shifts to more eastward forcing in the Nudged experiments (negative values in Control-Nudged), which aligns with the observed westerly shift in winds. MRI shows minimal changes in wind and GWD.

The corresponding figures showing the QBO phase composite of meridional advection, vertical advection and EPD are provided in the supplementary (figure S4). Similar to the GWD term, the vertical advection changes show a modulation by the QBO but they generally oppose the GWD forcing (figure S4). As a result of this, the maximum zonal winds changes in the Nudged experiments tend to occur when the vertical advection changes are near zero and GWD changes are still high. EPD and meridional advection changes in most models do not show any modulation by QBO phase.

4 Summary and Discussion

This study investigated whether biases in the SAO within various current climate models can be reduced when biases in the QBO are corrected. Ten models participating in the QBOi Phase 2 were analyzed. Each model had three ensemble-members for two experiments analysed: the Control and Nudged experiments. The Control experiments, in which the models were allowed to run freely, was used to assess the baseline SAO behaviour. The Nudged experiments, where the zonal-mean zonal winds at QBO altitude were nudged towards the ERA5 zonal-mean winds, were used to examine how the SAO is affected when the QBO biases are reduced.

As found in QBOi phase 1 (Smith et al., 2022), all the QBOi phase 2 models have an easterly bias at 1 hPa as compared to reanalysis. Correcting the QBO biases generally reduced this overall SAO bias by shifting the SAO more eastward, by more than 4 ms^{-1} in more than half of the models. In general, compared with the Control experiment, the Nudged experiment exhibits SAO westerlies that are stronger and more persistent, while SAO easterlies are weakened. However, the models

https://doi.org/10.5194/egusphere-2026-4135
Preprint. Discussion started: 22 July 2026

displayed a wide range in the strength of these responses. These ranged from very minimal change in the SAO winds (MRI with 6% change in time mean winds in Nudged compared to Control) to significant alterations that led to westerly winds completely dominating the SAO altitudes (ESM4 with 406% change in time mean winds in Nudged compared to Control). Consequently, the models were grouped together to gain a clearer understanding of these different responses. The study identified a group of models (the Similar group) that produced SAO amplitude and phase in the control simulations comparable to those of HadGEM3 discussed in Jaison et al. (2024b). These models demonstrated reasonable SAO amplitudes above 5 hPa, with alternating westerly and easterly winds peaking at altitudes higher than 1 hPa, along with a realistic annual cycle variability. In response to the QBO nudging, along with increased eastward GWD and decreased westward GWD, the SAO winds in these models became more westerly. The time-mean tropical-mean SAO zonal winds became more westerly by between 23% and 57% compared to the Control experiments in these models. These models also showed that the largest improvements in SAO occurred during periods when the QBO was in its westerly phase (based on 10 hPa QBO winds).

A Distinct group of models was also defined, which exhibited features deviating from those of HadGEM3 and showed inconsistent responses to the QBO nudging. CAS-ESM, E3SM and ESM4, members of this group, showed the most drastic changes in their Nudged experiments. All three models were identified to have a highly biased QBO profile, with no QBO at all in E3SM. The SAO in these models were also very different to reanalysis, either lacking the westerly winds in the SAO second cycle or having an incorrect annual cycle within the SAO. While nudging generally shifted the SAO winds toward more westerlies, this did not consistently result in improved SAO variability. GWD played a crucial role in these models as well, however, further analysis of these models is required to fully understand why they show such different responses. The remaining model in the Distinct group, MRI, showed little to no response at SAO altitudes to the QBO nudging, as the QBO changes were also minimal.

Examination of the TEM forcing terms showed that changes in resolved wave forcing in response to nudging towards more realistic QBO winds were very small and had limited impact on modifying the SAO. Instead, the dominant contributor to improvements in the SAO representation came from changes in GWD i.e. via the parameterization scheme for unresolved waves. The study therefore suggests that while improving the model representation of the QBO winds is likely to improve the representation of the SAO through improved filtering of waves reaching the SAO altitudes, deficiencies remain in the representation of tropical wave forcing contributing to the SAO. Improvements in both resolved and parameterized waves could further improve the SAO. For example, observational confirmation for the gravity wave spectrum could help determine if an emphasis on high-frequency waves, that are unfiltered at QBO altitude, could lead to further improvements of the SAO. Some models might also need improvements to the extra-tropical wave forcing, since the easterly phases are also not well simulated. Nevertheless, we note that the study is limited by the lack of direct observations at the SAO altitudes, and as nudging is an artificial forcing, in our case applied to a specific region of the atmosphere, there could be induced effects that we are unaware of. While zonal-mean nudging is suggested to have fewer unrealistic effects, models that use full-field nudging are more likely to restrict the free evolution of waves. It is envisaged that in the future, assuming direct stratospheric observations of wind become available through targeted satellite missions, more accurate information about the SAO forcing terms could be obtained for comparisons.

Code and data availability

The QBOi data archive was kindly hosted by the NERC Centre for Environmental Data Analysis (CEDA), UK, and processing was performed on the JASMIN infrastructure. MERRA-2 datasets used in this study are available at the Global Modeling and Assimilation Office (GMAO, 2015, https://doi.org/10.5067/SUOQESM06LPK).

Author contributions

AMJ, LJG and SO designed the study. AMJ performed data curation, formal analysis, visualization and writing (original text, reviewing and editing). LJG and SO provided supervision, reviewing and editing.
MA, ZC, DCH, KH, AMJ, YK, JK, PL, FL, YL, HN, NR, FS, IS, SWS, QT, SW, JX, KY: Setting up individual models, running the experiments, and provided data to the NERC CEDA archive, reviewing the manuscript. AKS: reviewing the manuscript. JAA, NB, SO, YK and JHR designed the QBOi phase 2 experiments and reviewed the manuscript.

Competing interests

JA serves as co-editor for the special issue to which this paper belongs. The remaining authors declare that they have no conflict of interest.

Acknowledgements

The authors acknowledge with thanks the UK Centre for Environmental Data Analysis (CEDA) and World Climate Research Programme (WCRP) Atmospheric Processes And their Role in Climate (APARC) for supporting the QBOi project. The authors gratefully acknowledge Monsoon2, a collaborative High-Performance Computing facility funded by the Met Office and the Natural Environment Research Council, which enabled some of the model simulations used in this study. MIROC6.1 simulations were performed using the Earth Simulator at JAMSTEC. FS thanks Paolo Davini for support in setting up the simulations of the EC-Earth3 model and acknowledges computing and archive resources provided by an ECMWF Special Project.

Financial support

AMJ was funded by an Oxford-Richards Graduate Scholarship. LJG and SO were supported by UK Research and Innovation (UKRI) and the Natural Environment Research Council (NERC) through their funding of the National Centre for Atmospheric Science (NCAS) and the CANARI programme. Y.L. was supported by the National Natural Science Foundation of China (42275056). QT and JX acknowledge support from the Earth and Environmental System Modeling (E3SM) project, funded by the U.S. Department of Energy (DOE), Office of Science, Office of Biological and Environmental Research (BER) through the Earth System Model Development (ESMD) program area. QT acknowledges grant support from the U.S. DOE BER's Regional and Global Model Analysis (RGMA) program via SCW1813. Lawrence Livermore National Laboratory (LLNL) is operated by Lawrence Livermore National Security, LLC, for the U.S. DOE, National Nuclear Security Administration under Contract DE-AC52-07NA27344. JX was supported by the LLNL LDRD project 22-ERD-008 titled Multiscale Wildfire Simulation Framework and Remote Sensing. JX acknowledges RGMA component of the E3SM Program of the U.S. DOE BER via NSF interagency agreement 1844590. K.H., J.H.R., and N.R. were supported by the RGMA component of the E3SM Program of the U.S. DOE BER under LLNL subaward DE-AC52-07NA27344, Lawrence Berkeley National Lab subaward DE-AC02-05CH11231, and Pacific Northwest National Lab subaward DE-AC05-76RL01830. K.H., J.H.R., and N.R. were also supported by the National Science Foundation (NSF) National Center for Atmospheric Research, which is a major facility sponsored by NSF under Cooperative Agreement No. 1852977. SW was supported by JSPS KAKENHI Grant Number JP26K00773 and the MEXT Program for Advanced Studies of Climate Change Projection (SENTAN) Grant Number JPMXD0722681344. SWS and DCH were funded by the Korea Meteorological Administration Research and Development Program under Grant (RS-2025-02313090). ZC was funded by the National Natural Science Foundation of China (42405170) and the National Key Research and Development Program of China (2024YFF0809003) and was technically supported by the National Large Scientific and Technological Infrastructure—Earth System Numerical Simulation Facility in China (https://cstr.cn/31134.02.EL). YK was supported by Japan Society for Promotion of Science (JSPS) KAKENHI Grant Numbers 26K00773, 25K01058, and 23K22574 by the Environment Research and Technology Development Fund (JPMEERF20242001) of the Environmental Restoration and Conservation Agency of Japan, and by MEXT program for the advanced studies of climate change projection (SENTAN) Grant Number JPMXD0722680395.

References

Amodei, M., Pawson, S., Scaife, A. A., Langematz, U., Lahoz, W., Li, D. M., and Simon, P.: The SAO and Kelvin waves in the EuroGRIPS GCMS and the UK Met. Office analyses, Ann. Geophys., 19, 99–114, https://doi.org/10.5194/angeo-19-99-2001, 2001.

https://doi.org/10.5194/egusphere-2026-4135
Preprint. Discussion started: 22 July 2026

Andrews, D. G., Holton, J. R., and Leovy, C. B.: Chapter 3 - Basic Dynamics, in: Middle Atmosphere Dynamics, vol. 40, edited by: Andrews, D. G., Holton, J. R., and Leovy, C. B., Academic Press, 113–149, https://doi.org/https://doi.org/10.1016/B978-0-12-058575-5.50008-6, 1987.

Andrews, M. B., Knight, J. R., Scaife, A. A., Lu, Y., Wu, T., Gray, L. J., and Schenzinger, V.: Observed and Simulated Teleconnections Between the Stratospheric Quasi-Biennial Oscillation and Northern Hemisphere Winter Atmospheric Circulation, Journal of Geophysical Research: Atmospheres, 124, 1219–1232, https://doi.org/https://doi.org/10.1029/2018JD029368, 2019.

Anstey, J. A., Butchart, N., Hamilton, K., and Osprey, S. M.: The SPARC quasi-biennial oscillation initiative, Quarterly Journal of the Royal Meteorological Society, 148, 2020.

Anstey, J. A., Butchart, N., Osprey, S., Kawatani, Y., Hamilton, K., Richter, J. H., Stockdale, T., Andrews, M. B., Chai, Z., Davini, P., Hong, D.-C., Huang, K., Jaison, A. M., Kerzenmacher, T., Knight, J. R., Lin, P., Lott, F., Lu, Y., Naoe, H., Serva, F., Simpson, I., Son, S.-W., Tang, Q., Watanabe, S., Xie, J., and Yoshida, K.: Experiment design, nudging protocol, and models participating in Phase 2 of the APARC Quasi-Biennial Oscillation initiative (QBOi), EGUsphere, 2026, 1–38, https://doi.org/10.5194/egusphere-2026-1165, 2026.

Antonita, T. M., Ramkumar, G., Kumar, K. K., Appu, K. S., and Nambhoodiri, K. V. S.: A quantitative study on the role of gravity waves in driving the tropical Stratospheric Semiannual Oscillation, Journal of Geophysical Research: Atmospheres, 112, https://doi.org/https://doi.org/10.1029/2006JD008250, 2007.

Baldwin, M. P., Gray, L. J., Dunkerton, T. J., Hamilton, K., Haynes, P. H., Randel, W. J., Holton, J. R., Alexander, M. J., Hirota, I., Horinouchi, T., Jones, D. B. A., Kinnersley, J. S., Marquardt, C., Sato, K., and Takahashi, M.: The quasi-biennial oscillation, Reviews of Geophysics, 39, 179–229, https://doi.org/https://doi.org/10.1029/1999RG000073, 2001.

Burrage, M. D., Vincent, R. A., Mayr, H. G., Skinner, W. R., Arnold, N. F., and Hays, P. B.: Long-term variability in the equatorial middle atmosphere zonal wind, Journal of Geophysical Research: Atmospheres, 101, 12847–12854, https://doi.org/https://doi.org/10.1029/96JD00575, 1996.

Bushell, A. C., Anstey, J. A., Butchart, N., Kawatani, Y., Osprey, S. M., Richter, J. H., Serva, F., Braesicke, P., Cagnazzo, C., Chen, C.-C., Chun, H.-Y., Garcia, R. R., Gray, L. J., Hamilton, K., Kerzenmacher, T., Kim, Y.-H., Lott, F., McLandress, C., Naoe, H., Scinocca, J., Smith, A. K., Stockdale, T. N., Versick, S., Watanabe, S., Yoshida, K., and Yukimoto, S.: Evaluation of the Quasi-Biennial Oscillation in global climate models for the SPARC QBO-initiative, Quarterly Journal of the Royal Meteorological Society, 148, 1459–1489, https://doi.org/https://doi.org/10.1002/qj.3765, 2022.

Butchart, N., Anstey, J. A., Hamilton, K., Osprey, S., McLandress, C., Bushell, A. C., Kawatani, Y., Kim, Y.-H., Lott, F., Scinocca, J., Stockdale, T. N., Andrews, M., Bellprat, O., Braesicke, P., Cagnazzo, C., Chen, C.-C., Chun, H.-Y., Dobrynin, M., Garcia, R. R., Garcia-Serrano, J., Gray, L. J., Holt, L., Kerzenmacher, T., Naoe, H., Pohlmann, H., Richter, J. H., Scaife, A. A., Schenzinger, V., Serva, F., Versick, S., Watanabe, S., Yoshida, K., and Yukimoto, S.: Overview of experiment design and comparison of models participating in phase 1 of the SPARC Quasi-Biennial Oscillation initiative (QBOi), Geosci. Model Dev., 11, 1009–1032, https://doi.org/10.5194/gmd-11-1009-2018, 2018.

https://doi.org/10.5194/egusphere-2026-4135
Preprint. Discussion started: 22 July 2026

Butchart, N., Andrews, M. B., and Jones, C. D.: QBO Phase Synchronization in CMIP6 Historical Simulations Attributed to Ozone Forcing, Geophys. Res. Lett., 50, e2023GL104401, https://doi.org/https://doi.org/10.1029/2023GL104401, 2023.

Deepa, V., Ramkumar, G., and Krishna Murthy, B. V: Gravity waves observed from the Equatorial Wave Studies (EWS) campaign during 1999 and 2000 and their role in the generation of stratospheric semiannual oscillations, Ann. Geophys., 24, 2481–2491, https://doi.org/10.5194/angeo-24-2481-2006, 2006.

Delisi, D. P. and Dunkerton, T. J.: Seasonal Variation of the Semiannual Oscillation, Journal of Atmospheric Sciences, 45, 2772–2787, https://doi.org/10.1175/1520-0469(1988)045<2772:SVOTSO>2.0.CO;2, 1988.

Döscher, R., Acosta, M., Alessandri, A., Anthoni, P., Arsouze, T., Bergman, T., Bernardello, R., Boussetta, S., Caron, L.-P., Carver, G., Castrillo, M., Catalano, F., Cvijanovic, I., Davini, P., Dekker, E., Doblas-Reyes, F. J., Docquier, D., Echevarria, P., Fladrich, U., Fuentes-Franco, R., Gröger, M., v. Hardenberg, J., Hieronymus, J., Karami, M. P., Keskinen, J.-P., Koenigk, T., Makkonen, R., Massonnet, F., Ménégoz, M., Miller, P. A., Moreno-Chamarro, E., Nieradzik, L., van Noije, T., Nolan, P., O'Donnell, D., Ollinaho, P., van den Oord, G., Ortega, P., Prims, O. T., Ramos, A., Reerink, T., Rousset, C., Ruprich-Robert, Y., Le Sager, P., Schmith, T., Schrödner, R., Serva, F., Sicardi, V., Sloth Madsen, M., Smith, B., Tian, T., Tourigny, E., Uotila, P., Vancoppenolle, M., Wang, S., Wårlind, D., Willén, U., Wyser, K., Yang, S., Yepes-Arbós, X., and Zhang, Q.: The EC-Earth3 Earth system model for the Coupled Model Intercomparison Project 6, Geosci. Model Dev., 15, 2973–3020, https://doi.org/10.5194/gmd-15-2973-2022, 2022.

Dunkerton, T.: On the Role of the Kelvin Wave in the Westerly Phase of the Semiannual Zonal Wind Oscillation, Journal of Atmospheric Sciences, 36, 32–41, https://doi.org/10.1175/1520-0469(1979)036<0032:OTROTK>2.0.CO;2, 1979.

Dunkerton, T. J. and Delisi, D. P.: Interaction of the quasi-biennial oscillation and stratopause semiannual oscillation, Journal of Geophysical Research: Atmospheres, 102, 26107–26116, https://doi.org/https://doi.org/10.1029/96JD03678, 1997.

Ern, M., Diallo, M., Preusse, P., Mlynczak, M. G., Schwartz, M. J., Wu, Q., and Riese, M.: The semiannual oscillation (SAO) in the tropical middle atmosphere and its gravity wave driving in reanalyses and satellite observations, Atmos. Chem. Phys., 21, 13763–13795, https://doi.org/10.5194/acp-21-13763-2021, 2021.

Garcia, R. R. and Sassi, F.: Modulation of the mesospheric semiannual oscillation by the quasibiennial oscillation, Earth, Planets and Space, 51, 563–569, https://doi.org/10.1186/BF03353215, 1999.

Garcia, R. R., Dunkerton, T. J., Lieberman, R. S., and Vincent, R. A.: Climatology of the semiannual oscillation of the tropical middle atmosphere, Journal of Geophysical Research: Atmospheres, 102, 26019–26032, https://doi.org/https://doi.org/10.1029/97JD00207, 1997.

Garfinkel, C. I., Gerber, E. P., Shamir, O., Rao, J., Jucker, M., White, I., and Paldor, N.: A QBO Cookbook: Sensitivity of the Quasi-Biennial Oscillation to Resolution, Resolved Waves, and Parameterized Gravity Waves, J. Adv. Model. Earth Syst., 14, e2021MS002568, https://doi.org/https://doi.org/10.1029/2021MS002568, 2022.

Gelaro, R., McCarty, W., Suárez, M. J., Todling, R., Molod, A., Takacs, L., Randles, C. A., Darmenov, A., Bosilovich, M. G., Reichle, R., Wargan, K., Coy, L., Cullather, R., Draper, C., Akella, S., Buchard, V., Conaty, A., da Silva, A. M., Gu, W.,

https://doi.org/10.5194/egusphere-2026-4135
Preprint. Discussion started: 22 July 2026

Kim, G.-K., Koster, R., Lucchesi, R., Merkova, D., Nielsen, J. E., Partyka, G., Pawson, S., Putman, W., Rienecker, M., Schubert, S. D., Sienkiewicz, M., and Zhao, B.: The Modern-Era Retrospective Analysis for Research and Applications, Version 2 (MERRA-2), J. Clim., 30, 5419–5454, https://doi.org/10.1175/JCLI-D-16-0758.1, 2017.

Golaz, J.-C., Van Roekel, L. P., Zheng, X., Roberts, A. F., Wolfe, J. D., Lin, W., Bradley, A. M., Tang, Q., Maltrud, M. E., Forsyth, R. M., Zhang, C., Zhou, T., Zhang, K., Zender, C. S., Wu, M., Wang, H., Turner, A. K., Singh, B., Richter, J. H., Qin, Y., Petersen, M. R., Mametjanov, A., Ma, P.-L., Larson, V. E., Krishna, J., Keen, N. D., Jeffery, N., Hunke, E. C., Hannah, W. M., Guba, O., Griffin, B. M., Feng, Y., Engwirda, D., Di Vittorio, A. V, Dang, C., Conlon, L. M., Chen, C.-C.-J., Brunke, M. A., Bisht, G., Benedict, J. J., Asay-Davis, X. S., Zhang, Y., Zhang, M., Zeng, X., Xie, S., Wolfram, P. J., Vo, T., Veneziani, M., Tesfa, T. K., Sreepathi, S., Salinger, A. G., Reeves Eyre, J. E. J., Prather, M. J., Mahajan, S., Li, Q., Jones, P. W., Jacob, R. L., Huebler, G. W., Huang, X., Hillman, B. R., Harrop, B. E., Foucar, J. G., Fang, Y., Comeau, D. S., Caldwell, P. M., Bartoletti, T., Balaguru, K., Taylor, M. A., McCoy, R. B., Leung, L. R., and Bader, D. C.: The DOE E3SM Model Version 2: Overview of the Physical Model and Initial Model Evaluation, J. Adv. Model. Earth Syst., 14, e2022MS003156, https://doi.org/https://doi.org/10.1029/2022MS003156, 2022.

Gray, L. J. and Pyle, J. A.: The semi-annual oscillation and equatorial tracer distributions, Quarterly Journal of the Royal Meteorological Society, 112, 387–407, https://doi.org/https://doi.org/10.1002/qj.49711247207, 1986.

Gray, L. J., Brown, M. J., Knight, J., Andrews, M., Lu, H., O'Reilly, C., and Anstey, J.: Forecasting extreme stratospheric polar vortex events, Nat. Commun., 11, 4630, https://doi.org/10.1038/s41467-020-18299-7, 2020.

Hamilton, K. and Mahlman, J. D.: General Circulation Model Simulation of the Semiannual Oscillation of the Tropical Middle Atmosphere, Journal of Atmospheric Sciences, 45, 3212–3235, https://doi.org/10.1175/1520-0469(1988)045<3212:GCMSOT>2.0.CO;2, 1988.

Hersbach, H., Bell, B., Berrisford, P., Hirahara, S., Horányi, A., Muñoz-Sabater, J., Nicolas, J., Peubey, C., Radu, R., Schepers, D., Simmons, A., Soci, C., Abdalla, S., Abellan, X., Balsamo, G., Bechtold, P., Biavati, G., Bidlot, J., Bonavita, M., De Chiara, G., Dahlgren, P., Dee, D., Diamantakis, M., Dragani, R., Flemming, J., Forbes, R., Fuentes, M., Geer, A., Haimberger, L., Healy, S., Hogan, R. J., Hólm, E., Janisková, M., Keeley, S., Laloyaux, P., Lopez, P., Lupu, C., Radnoti, G., de Rosnay, P., Rozum, I., Vamborg, F., Villaume, S., and Thépaut, J.-N.: The ERA5 global reanalysis, Quarterly Journal of the Royal Meteorological Society, 146, 1999–2049, https://doi.org/https://doi.org/10.1002/qj.3803, 2020.

Hirota, I.: Equatorial Waves in the Upper Stratosphere and Mesosphere in Relation to the Semiannual Oscillation of the Zonal Wind, Journal of Atmospheric Sciences, 35, 714–722, https://doi.org/10.1175/1520-0469(1978)035<0714:EWITUS>2.0.CO;2, 1978.

Hitchman, M. H. and Leovy, C. B.: Estimation of the Kelvin Wave Contribution to the Semiannual oscillation, Journal of Atmospheric Sciences, 45, 1462–1475, https://doi.org/10.1175/1520-0469(1988)045<1462:EOTKWC>2.0.CO;2, 1988.

Holton, J. R. and Wehrbein, W. M.: A numerical model of the zonal mean circulation of the middle atmosphere, Pure Appl. Geophys., 118, 284–306, https://doi.org/10.1007/BF01586455, 1980.

https://doi.org/10.5194/egusphere-2026-4135
Preprint. Discussion started: 22 July 2026

Hopkins, R. H.: Evidence of Polar-Tropical Coupling in Upper Stratospheric Zonal Wind Anomalies, Journal of Atmospheric Sciences, 32, 712–719, https://doi.org/10.1175/1520-0469(1975)032<0712:EOPTCI>2.0.CO;2, 1975.

Jackson, D. R. and Gray, L. J.: Simulation of the semi-annual oscillation of the equatorial middle atmosphere using the Extended UGAMP General Circulation Model, Quarterly Journal of the Royal Meteorological Society, 120, 1559–1588, https://doi.org/https://doi.org/10.1002/qj.49712052007, 1994.

Jaison, A. M., Gray, L. J., Osprey, S., Smith, A. K., and Garcia, R. R.: A momentum budget study of the semi-annual oscillation in the Whole Atmosphere Community Climate Model, Quarterly Journal of the Royal Meteorological Society, n/a, 1–22, https://doi.org/https://doi.org/10.1002/qj.4782, 2024a.

Jaison, A. M., Gray, L. J., Osprey, S. M., Knight, J. R., and Andrews, M. B.: Role of the quasi-biennial oscillation in alleviating biases in the semi-annual oscillation, Weather and Climate Dynamics, 5, 1489–1504, https://doi.org/10.5194/wcd-5-1489-2024, 2024b.

Kawatani, Y., Hamilton, K., Miyazaki, K., Fujiwara, M., and Anstey, J. A.: Representation of the tropical stratospheric zonal wind in global atmospheric reanalyses, Atmos. Chem. Phys., 16, 6681–6699, https://doi.org/10.5194/acp-16-6681-2016, 2016.

Kawatani, Y., Hirooka, T., Hamilton, K., Smith, A. K., and Fujiwara, M.: Representation of the equatorial stratopause semiannual oscillation in global atmospheric reanalyses, Atmos. Chem. Phys., 20, 9115–9133, https://doi.org/10.5194/acp-20-9115-2020, 2020.

Meyer, W. D.: A Diagnostic Numerical Study of the Semiannual Variation of the Zonal Wind in the Tropical Stratosphere and Mesosphere, Journal of Atmospheric Sciences, 27, 820–830, https://doi.org/10.1175/1520-0469(1970)027<0820:ADNSOT>2.0.CO;2, 1970.

Molod, A., Takacs, L., Suarez, M., and Bacmeister, J.: Development of the GEOS-5 atmospheric general circulation model: evolution from MERRA to MERRA2, Geosci. Model Dev., 8, 1339–1356, https://doi.org/10.5194/gmd-8-1339-2015, 2015.

Peña-Ortiz, C., Schmidt, H., Giorgetta, M. A., and Keller, M.: QBO modulation of the semiannual oscillation in MAECHAM5 and HAMMONIA, Journal of Geophysical Research: Atmospheres, 115, https://doi.org/https://doi.org/10.1029/2010JD013898, 2010.

Quiroz, R. S. and Miller, A.: NOTE ON THE SEMI-ANNUAL WIND VARIATION IN THE EQUATORIAL STRATOSPHERE, Mon. Weather Rev., 95, 635–641, https://doi.org/10.1175/1520-0493(1967)095<0635:NOTSAW>2.3.CO;2, 1967.

Rao, J., Garfinkel, C. I., and White, I. P.: Impact of the Quasi-Biennial Oscillation on the Northern Winter Stratospheric Polar Vortex in CMIP5/6 Models, J. Clim., 33, 4787–4813, https://doi.org/https://doi.org/10.1175/JCLI-D-19-0663.1, 2020.

Ray, E. A., Alexander, M. J., and Holton, J. R.: An analysis of the structure and forcing of the equatorial semiannual oscillation in zonal wind, Journal of Geophysical Research: Atmospheres, 103, 1759–1774, https://doi.org/https://doi.org/10.1029/97JD02679, 1998.

https://doi.org/10.5194/egusphere-2026-4135
Preprint. Discussion started: 22 July 2026

Reed, R. J.: Zonal wind behavior in the equatorial stratosphere and lower mesosphere, Journal of Geophysical Research (1896-1977), 71, 4223–4233, https://doi.org/https://doi.org/10.1029/JZ071i018p04223, 1966.

Richter, J. H. and Garcia, R. R.: On the forcing of the Mesospheric Semi-Annual Oscillation in the Whole Atmosphere Community Climate Model, Geophys. Res. Lett., 33, https://doi.org/https://doi.org/10.1029/2005GL024378, 2006.

Serva, F., Christiansen, B., Davini, P., von Hardenberg, J., van den Oord, G., Reerink, T. J., Wyser, K., and Yang, S.: Changes in Stratospheric Dynamics Simulated by the EC-Earth Model From CMIP5 to CMIP6, J. Adv. Model. Earth Syst., 16, e2023MS003756, https://doi.org/https://doi.org/10.1029/2023MS003756, 2024.

Smith, A. K., Garcia, R. R., Moss, A. C., and Mitchell, N. J.: The Semiannual Oscillation of the Tropical Zonal Wind in the Middle Atmosphere Derived from Satellite Geopotential Height Retrievals, J. Atmos. Sci., 74, 2413–2425, https://doi.org/10.1175/JAS-D-17-0067.1, 2017.

Smith, A. K., Holt, L. A., Garcia, R. R., Anstey, J. A., Serva, F., Butchart, N., Osprey, S., Bushell, A. C., Kawatani, Y., Kim, Y.-H., Lott, F., Braesicke, P., Cagnazzo, C., Chen, C.-C., Chun, H.-Y., Gray, L., Kerzenmacher, T., Naoe, H., Richter, J., Versick, S., Schenzinger, V., Watanabe, S., and Yoshida, K.: The equatorial stratospheric semiannual oscillation and time-mean winds in QBOi models, Quarterly Journal of the Royal Meteorological Society, 148, 1593–1609, https://doi.org/https://doi.org/10.1002/qj.3690, 2022.

Smith, A. K., Gray, L. J., and Garcia, R. R.: Evidence for the Influence of the Quasi-Biennial Oscillation on the Semiannual Oscillation in the Tropical Middle Atmosphere, J. Atmos. Sci., 80, 1755–1769, https://doi.org/https://doi.org/10.1175/JAS-D-22-0255.1, 2023.